

# Nonaxisymmetric Neutral Modes of Rotating Relativistic Stars

Nikolaos Stergioulas, John L. Friedman

University of Wisconsin-Milwaukee, P.O. Box 413, Milwaukee, WI 53201

niksterg@eexi.gr, friedman@thales.phys.uwm.edu

Received \_\_\_\_\_; accepted \_\_\_\_\_

Submitted to the Astrophysical Journal

arXiv:gr-qc/9705056v2 22 May 1997

## ABSTRACT

We study nonaxisymmetric perturbations of rotating relativistic stars, modeled as perfect-fluid equilibria. Instability to a mode with angular dependence  $\exp(im\phi)$  sets in when the frequency of the mode vanishes. The locations of these zero-frequency modes along sequences of rotating stars are computed in the framework of general relativity. We consider models of uniformly rotating stars with polytropic equations of state, finding that the relativistic models are unstable to nonaxisymmetric modes at significantly smaller values of rotation than in the Newtonian limit. Most strikingly, the  $m=2$  bar mode can become unstable even for soft polytropes of index  $N \leq 1.3$ , while in Newtonian theory it becomes unstable only for stiff polytropes of index  $N \leq 0.808$ . If rapidly rotating neutron stars are formed by the accretion-induced collapse of white dwarfs, instability associated with these nonaxisymmetric, gravitational-wave driven modes may set an upper limit on neutron-star rotation. Consideration is restricted to perturbations that correspond to polar perturbations of a spherical star. A study of axial perturbations is in progress.

*Subject headings:* ...

## 1. Introduction

Rotating perfect-fluid equilibria are unstable to nonaxisymmetric instabilities driven by gravitational radiation. Although apparently damped by viscosity in neutron stars cold enough to have a superfluid interior, the instability may play a role in limiting the maximum rotation of newly formed neutron stars. In particular, if rapidly rotating neutron stars with weak magnetic fields form in the accretion-induced collapse of some white dwarfs (or the core-collapse of some stars), the instability may set an upper limit on rotation more stringent than the Kepler frequency – the frequency of a satellite in circular orbit at the star’s equator.

Prior to the present work, the onset of the nonaxisymmetric instability had been computed only in the Newtonian limit and estimated in the first post-Newtonian approximation and in a slow-rotation approximation.<sup>1</sup> The first fully relativistic computation is presented here (and in Stergioulas’ PhD thesis (1996)).

That stars can be unstable to gravitational radiation was first found by Chandrasekhar (1970), who considered the  $m = 2$  modes for Maclaurin spheroids (uniform density rotating stars) in a Newtonian context. Friedman & Schutz (1975, 1978a, 1978b), show that this instability also appears in compressible stars and that all rotating “stars” (rotating self-gravitating perfect-fluid configurations) are generically unstable to the emission of gravitational radiation. Even for slowly rotating models there will always be a polar mode of high enough mode number  $m$  (equivalently, of short enough wavelength) that is unstable.

---

<sup>1</sup>After this was written, we received a preprint by Yoshida and Eriguchi (1997) computing instability points using a Cowling approximation in general relativity. This is an approximation that ignores changes in the gravitational potential, and it should be accurate for large- $m$  modes.

For a perfect fluid, a nonaxisymmetric mode becomes unstable when its frequency vanishes in the inertial frame, i.e., with respect to an observer at infinity. This occurs when a star rotates fast enough that an inertial observer sees that a counterrotating mode becomes corotating with the star. The amplitude of the perturbation then grows with time, making the star unstable.

Realistic neutron stars are viscous, and the presence of viscosity will shift the onset of instability. Work by Lindblom & Mendell (1995) (see also Ipser & Lindblom 1991a,b; Yoshida & Eriguchi 1995) shows that viscosity will damp out the instability once the temperature is low enough that the interior is superfluid. A window apparently remains, of temperatures less than about  $10^9$  K and greater than about  $10^{10}$  K, where the instability will affect a sufficiently rapidly rotating neutron star as it cools down after its birth. In the Newtonian limit, it appears that only the  $l = m \leq 5$  modes are not damped out by viscosity and the  $l = 4$  mode apparently sets the most stringent limit on the maximum angular velocity; the critical angular velocity is about 90 % to 95 % of the Kepler limit. Old neutron stars, spun-up by accretion, may be too cold to be subject to the gravitational radiation driven instability.

A surprise, recently pointed out by Andersson (Andersson 1997; Friedman and Morsink 1997) is that axial modes for all values of  $m$  will be unstable for perfect-fluid models with arbitrarily slow rotation. In a spherical star, axial perturbations are time-independent convective currents that do not change the density and pressure of the star and do not couple to gravitational waves. For rotating stars, their growth time  $\tau$  is proportional to a high power of  $\Omega$  (rough arguments appear to imply  $\tau \propto \Omega^{-4-2m}$ ), and viscosity will again presumably enforce stability except for hot, rapidly rotating neutron stars.

The onset of the nonaxisymmetric instability for several modes in rotating polytropes has been computed in the Newtonian limit by Imamura, Friedman & Durisen (1985)

using a Lagrangian variational principle and by Managan (1985) and Ipser & Lindblom (1990) using an Eulerian variational principle constructed by Ipser & Managan (1985). Cutler (1991), Cutler & Lindblom (1992) and Lindblom (1995) estimate the correction to first post-Newtonian order. Weber et al (1991) provide an estimate in a relativistic, slow-rotation approximation. Since neutron stars are relativistic objects, relativity must have a significant effect on the onset of instability. The post-Newtonian analysis suggests that, for a given equation of state (EOS) and a given mode  $l$ , the ratio  $\Omega_c/\Omega_k$  of the critical angular velocity where the mode becomes unstable to the maximum allowed angular velocity (the Kepler frequency  $\Omega_k$ ) decreases as the neutron star becomes more relativistic. Thus, nonaxisymmetric instabilities set a more stringent limit on the maximum angular velocity than Newtonian theory suggests.

In this paper, we report the first computation of zero-frequency modes of rotating relativistic stars. Polytropes of index  $N = 1.0, 1.5$  and  $2.0$  are considered, and attention is restricted to the fundamental (f)  $l = m \leq 5$  modes, since these are the ones that are most likely to participate in limiting the maximum angular velocity of neutron stars. It is shown that the critical angular velocities of relativistic stars are considerably lower than the corresponding Newtonian estimates. As a result, the  $m = 2$  bar mode can become unstable for much softer ( $N < 1.3$ ) polytropes than in the Newtonian limit. This is expected to hold true for most realistic EOSs since they have an effective index  $N < 1.0$ . Thus, depending on the equation of state and the effect of viscosity, the  $m = 2$  mode may participate in setting the upper limit on rotation for rapidly rotating neutron stars created by the accretion-induced collapse of white dwarfs.

In forthcoming work we plan to include the effect of viscosity on the critical angular velocities and extend our method to  $N < 1.0$  polytropes and to realistic equations of state.

## 2. The Equilibrium Configurations

The spacetime of a rotating relativistic star in equilibrium can be described by the stationary, axisymmetric metric of the form

$$ds^2 = -e^{2\nu} dt^2 + e^{2\psi} (d\phi - \omega dt)^2 + e^{2\alpha} (dr^2 + r^2 d\theta^2), \quad (1)$$

(for a review see Friedman & Ipser (1992) ).

In (1), as in the rest of this paper, gravitational units ( $c = 1$ ,  $G = 1$ ) are employed. The metric involves four independent equilibrium metric potentials  $\nu, \psi, \alpha$  and  $\omega$  which are functions of  $r$  and  $\theta$  only. We assume uniform rotation,  $\Omega = \text{constant}$ , where  $\Omega$  is the angular velocity of the star. The matter is assumed to be a perfect fluid at zero temperature, described by a polytropic equation of state, for which the energy density  $\epsilon$ , pressure  $P$  and number density  $n$  satisfy the relations

$$P = Kn^{1+1/N}, \quad (2)$$

$$\epsilon = nm_{\text{B}} + NKn^{1+1/N}, \quad (3)$$

where  $K$  is a constant,  $m_{\text{B}}$  is the rest mass per baryon and  $N$  is the polytropic index, related to the adiabatic index  $\gamma$  by

$$\gamma = \frac{d \ln P}{d \ln n} = \frac{\epsilon + P}{P} \frac{dP}{d\epsilon} = 1 + \frac{1}{N}. \quad (4)$$

The stress-energy tensor for a perfect fluid is

$$T^{ab} = (\epsilon + P)u^a u^b + P g^{ab}, \quad (5)$$

where the equilibrium 4-velocity  $u^a$  is given by

$$u^a = \frac{e^{-\nu}}{\sqrt{1-v^2}}(t^a + \Omega\phi^a), \quad (6)$$

with

$$v = (\Omega - \omega)e^{\psi-\nu}, \quad (7)$$

the fluid velocity with respect to a local zero-angular-momentum observer. We have denoted by  $t^a$  and  $\phi^a$  the Killing vectors  $\partial_t$  and  $\partial_\phi$  associated with the time and rotational symmetries of the metric.

An equilibrium model satisfies the field equation,

$$R_{ab} = 8\pi\left(T_{ab} - \frac{1}{2}g_{ab}T\right), \quad (8)$$

and the implied equation of energy conservation

$$u_b\nabla_a T^{ab} = 0 \implies u^a\nabla_a\epsilon = -(\epsilon + P)\nabla_a u^a. \quad (9)$$

and Euler equation

$$q^c{}_b\nabla_a T^{ab} = 0 \implies u^a\nabla_a u^b = \frac{q^{bc}\nabla_c P}{\epsilon + P}, \quad (10)$$

Here  $q^{ab} = g^{ab} + u^a u^b$  is the projection of the metric tensor orthogonal to the 4-velocity.

Numerical equilibrium models are constructed by a numerical code (Stergioulas & Friedman (1995) ) that implements the Cook, Shapiro & Teukolsky (1994) version of the KEH method (Komatsu, Eriguchi & Hachisu (1989) ). Our code has been shown to be accurate in an extensive comparison with other existing codes (Eriguchi *et al.* (1996) ). The field equations are solved on a 2-dimensional grid that is uniform in  $\mu \equiv \cos\theta$  and in the radial coordinate

$$s = r/(r + r_e), \tag{11}$$

which compactifies the region  $r = 0$  to  $+\infty$  to the finite region  $s = 0$  to 1 ( $r_e$  is the value of the coordinate  $r$  at the equator). This is important, because the gravitational potentials have a nonnegligible value even far from a relativistic star; and it also simplifies the implementation of boundary conditions in the construction of both the equilibrium and the perturbed configurations. Note that the equator of the star is always at  $s = 0.5$ , so that (for a nonrotating star) half of the radial grid-points are inside the star and the other half are outside.

We define dimensionless quantities by setting  $G = c = 1$  and by fixing the length scale. If we define

$$\tilde{K} = \frac{K}{m_B^{1+1/N}}, \tag{12}$$

then  $\tilde{K}^{N/2}$  can be used as the fundamental length scale. Dimensionless quantities will be denoted as  $\bar{\epsilon}$ ,  $\bar{\Omega}$  etc. The dimensionless energy density and angular velocity are then

$$\bar{\epsilon} = \frac{\tilde{K}^N G}{c^4} \epsilon, \tag{13}$$

and

$$\bar{\Omega} = \frac{\tilde{K}^{N/2}}{c} \Omega. \tag{14}$$

In subsequent sections, numerical results will be reported using dimensionless quantities as defined above. *Note that the dimensionless quantities are independent of the polytropic constant  $K$ .*

### 3. The Perturbed Configurations

We will use an Eulerian formalism to describe fluid perturbations. The Eulerian perturbation in the metric tensor,

$$\delta g_{ab} \equiv h_{ab}, \quad (15)$$

can be determined by solving the perturbed field equations,

$$\delta R_{ab} = 8\pi(\delta T_{ab} - \frac{1}{2}g_{ab}\delta T - \frac{1}{2}h_{ab}T), \quad (16)$$

in a suitably chosen gauge. The perturbation in any other quantity is evaluated to first order in  $h_{ab}$ . The change in the Ricci tensor is then (see e.g. Wald 1984 )

$$\delta R_{ab} = \nabla_c \nabla_{(a} h^c{}_{b)} - \frac{1}{2}(\nabla_a \nabla_b h^c{}_c + \nabla^c \nabla_c h_{ab}), \quad (17)$$

where  $h^a{}_b = g^{ac}h_{cb}$ . Priou 1992 has explicitly computed the components of  $\delta R_{ab}$  for a stationary, axisymmetric background in its most general form (prior to any choice of gauge).

This allows us to directly use Priou's results with only the following modifications:

- i) since we are only interested in zero-frequency modes, we set the frequency of the mode and all time-derivatives equal to zero;
- ii) we rename Priou's functions, changing  $m$  to  $M$ ,  $l$  to  $L$  and  $\Omega$  to  $y$ , in order to avoid confusion with the indices  $l, m$  that characterize a mode and with the angular velocity  $\Omega$  of the equilibrium star; and
- iii) we choose a gauge as described in section 5.

The components of  $\delta R_{ab}$  in our gauge are displayed in Appendix A.

The perturbation of the stress-energy tensor is

$$\delta T_{ab} = u_a u_b (\delta \epsilon + \delta P) + (\epsilon + P)(u_a \delta u_b + u_b \delta u_a) + g_{ab} \delta P + P h_{ab}, \quad (18)$$

while the perturbation of its contraction is

$$\delta T = 3\delta P - \delta \epsilon, \quad (19)$$

The change in pressure and energy density can be expressed in terms of a single scalar function  $\delta U$ , defined implicitly by the relation

$$\delta P = (\epsilon + P) \left( \delta U + \frac{1}{2} u^a u^b h_{ab} \right). \quad (20)$$

For an adiabatic perturbation, we have

$$\delta \epsilon = \frac{(\epsilon + P)}{P\Gamma} \delta P, \quad (21)$$

and we will assume that the adiabatic index  $\Gamma$  of the perturbation be equal to the adiabatic index  $\Gamma_0$  of the equilibrium configuration, defined in (4).

In the perturbed relativistic Euler equations,

$$\delta(q^a{}_c \nabla_b T^{bc}) = 0, \quad (22)$$

the only derivatives of  $\delta u^a$  that occur are along the unperturbed fluid velocity  $u^a$ . For perturbations with harmonic  $t$ - and  $\phi$ -dependence, the equations are thus algebraic in  $\delta u^a$  and can be solved analytically (Ipser & Lindblom, 1992). The perturbed fluid velocity is given by

$$\delta u^a = i Q^{ab} \left[ \nabla_b \left( \delta U + \frac{1}{2} u^c u^d h_{cd} \right) - \delta F_b \right] + \frac{1}{2} u^a u^c u^d h_{cd}, \quad (23)$$

where

$$\delta F_a = q_a{}^b \left[ -u^c \nabla_c (h_{bd} u^d) + u^c u^d \nabla_b h_{cd} + u^c u^d h_{cd} \frac{\nabla_b P}{\epsilon + P} \right]. \quad (24)$$

The tensor  $Q^{ab}$  involves only equilibrium quantities and the frequency  $\sigma$  of the mode in a rotating frame; for the time-independent perturbations considered here,

$$\sigma = m\Omega. \quad (25)$$

Explicitly,

$$Q^{ab} = \frac{1}{D} \left[ (\sigma u^t)^2 q^{ab} - 2\omega^a \Omega^b + i\sigma u^t (2\hat{\phi}^b \epsilon^{ac} \Omega_c - \hat{\phi}^a \epsilon^{bc} \omega_c) \right]. \quad (26)$$

Here

$$u^t = u^a \nabla_a t = \left[ e^{2v} - e^{2\psi} (\Omega - \omega)^2 \right]^{1/2}; \quad (27)$$

the quantity

$$D = (\sigma u^t)^3 - 2\sigma u^t \Omega^a \omega_a \quad (28)$$

is the determinant of  $Q^{-1}$ ;  $\omega^a$  is the vorticity of the fluid,

$$\omega^a = \epsilon^{abcd} u_b \nabla_c u_d; \quad (29)$$

$\Omega^a$  is a generalization of the angular-velocity vector,

$$\Omega^a = \frac{1}{2} u^t \epsilon^{abcd} u_b (\nabla_c t_d + \Omega \nabla_c \phi_d); \quad (30)$$

$\hat{\phi}^a$  is the unit linear combination of the Killing fields that is orthogonal to  $u^a$ ,

$$\hat{\phi}^a = \frac{e^{-\psi-v}}{u^t} q^a{}_b \phi^b; \quad (31)$$

and the tensor  $\epsilon^{ab}$  is the volume element on the 2-surfaces orthogonal to the Killing trajectories

$$\epsilon^{ab} = \epsilon^{abcd} \hat{\phi}_c u_d. \quad (32)$$

The tensor  $Q^{ab}$  exists (and the perturbed Euler equations can be inverted) as long as the determinant in (28) does not vanish.

For completeness, we list components of  $u_a$ ,  $\omega^a$  and  $Q^{ab}$ . With  $u^t$  given by Eq. (27), we have

$$\begin{aligned} u_\phi &= u_a \phi^a = e^{2\psi} (\Omega - \omega) u^t; \\ \omega^r &= \frac{e^{-\psi-\nu-2\alpha}}{r(u^t)^2} \partial_\theta (u^t u_\phi) \\ \omega^\theta &= -\frac{e^{-\psi-\nu-2\alpha}}{r(u^t)^2} \partial_r (u^t u_\phi) \\ Q^{tt} &= \sigma^2 e^{-2\psi-2\nu} D^{-1} (u^t u_\phi)^2 \\ Q^{tr} &= -Q^{rt} = -i\sigma e^{-\psi-\nu} r \omega^\theta D^{-1} u^t u_\phi \\ Q^{t\theta} &= -Q^{\theta t} = -i\sigma e^{-\psi-\nu} r^{-1} \omega^r D^{-1} u^t u_\phi \\ Q^{t\phi} &= Q^{\phi t} = \frac{1 + \Omega u^t u_\phi}{u^t u_\phi} Q^{tt} \\ Q^{rr} &= D^{-1} [(\sigma u^t)^2 e^{-2\alpha} - (\omega^r)^2] \\ Q^{r\theta} &= -Q^{\theta r} = -D^{-1} \omega^r \omega^\theta \\ Q^{r\phi} &= -Q^{\phi r} = i\sigma e^{-\psi-\nu} r \omega^\theta D^{-1} (1 + \Omega u^t u_\phi) \\ Q^{\theta\theta} &= r^{-2} D^{-1} [(\sigma u^t)^2 e^{-2\alpha} - r^2 (\omega^\theta)^2] \\ Q^{\theta\phi} &= -Q^{\phi\theta} = -i\sigma e^{-\psi-\nu} r^{-1} \omega^r D^{-1} (1 + \Omega u^t u_\phi) \\ Q^{\phi\phi} &= \left( \frac{1 + \Omega u^t u_\phi}{u^t u_\phi} \right)^2 Q^{tt} \end{aligned}$$

The perturbed covariant fluid velocity is given by

$$\delta u_a = \delta u^b g_{ab} + u^b h_{ab}. \quad (33)$$

Through (20), (21), (23), (24) and the equation (33) for the perturbed covariant fluid velocity, the perturbation in the stress-energy tensor  $\delta T_{ab}$  is expressed entirely in terms of the perturbed metric  $h_{ab}$  and the scalar  $\delta U$ . Due to the lengthy substitutions involved, we used the algebraic program MAPLE to compute  $\delta u_a$  which was then substituted in  $\delta T_{ab}$ . The expressions for the components of  $\delta T_{ab}$  in the stationary, axisymmetric background are several pages long (for each component), and we do not display them here. These expressions, along with the components of  $\delta R_{ab}$ , are used to form the perturbed field equations (16). MAPLE is used to convert these expressions into numerical code for inclusion in an ANSI-C program.

The perturbed field equations determine  $h_{ab}$  for given  $\delta U$ . The scalar function  $\delta U$  is determined by an additional equation, the perturbed energy conservation equation

$$\delta(u_b \nabla_a T^{ab}) = 0. \quad (34)$$

which will be considered in section 8.

#### 4. Expansion in Spherical Harmonics

Because the equilibrium configuration is axisymmetric, linear perturbations of the star and geometry can be decomposed into a sum of terms with angular dependence  $e^{im\phi}$ . We expect that, as is the case for spherical stars, each discrete mode of a nonrotating, spherical model has a continuous extension to a mode for each rotating model with the same equation of state. Modes of spherical stars have angular dependence given by the tensor, vector and scalar harmonics associated with a given  $Y_l^m(\theta, \phi)$ . The corresponding mode of a rotating

model can thus be labeled by  $l$  and  $m$ ; but all harmonics  $Y_{l'}^m$ , with  $l' \geq l \geq m$  contribute to the mode.

Studies of rotating Newtonian stars find nonaxisymmetric instability sets in first along a sequence with increasing rotation for a reflection-invariant polar mode with  $l = m$ , the lowest value of  $l$  for a given  $m$ . We have, in this first numerical study, correspondingly restricted our consideration to perturbations invariant under reflection in the equatorial plane (under the diffeo  $\theta \rightarrow \pi - \theta$ )<sup>2</sup>.

The Eulerian perturbation in a reflection-symmetric,  $l = m$ , time-independent mode has the form

$$h_{tt}, h_{rr} \propto \sum_{l'=0}^{\infty} a_{m+2l'} Y_{m+2l'}^m \quad (35)$$

$$h_{tr} \propto \sum_{l'=0}^{\infty} i a_{m+2l'+2} Y_{m+2l'+2}^m \quad (36)$$

$$h_{t\mu} \propto \sum_{l'=0}^{\infty} \left( i a_{m+2l'+2} \Psi_{m+2l'+2, \mu}^m + b_{m+2l'+1} \Phi_{m+2l'+1, \mu}^m \right) \quad (37)$$

$$h_{r\mu} \propto \sum_{l'=0}^{\infty} \left( a_{m+2l'+2} \Psi_{m+2l'+2, \mu}^m + i b_{m+2l'+1} \Phi_{m+2l'+1, \mu}^m \right) \quad (38)$$

$$h_{\mu\nu} \propto \sum_{l'=0}^{\infty} \left( a_{m+2l'} \Phi_{m+2l', \mu\nu}^m + b_{m+2l'+2} \Psi_{m+2l'+2, \mu\nu}^m + i c_{m+2l'+1} \chi_{m+2l'+1, \mu\nu}^m \right) \quad (39)$$

where the  $a$ 's,  $b$ 's, and  $c$ 's are real coefficients, different for each component of  $h_{ab}$ . We have adopted the Regge-Wheeler (1957) notation for spherical harmonics:

---

<sup>2</sup>Recall that if a vector  $v^a$  is invariant under the diffeo  $\theta \rightarrow \pi - \theta$  its components  $v^r = v^a \nabla_a r$ ,  $v^t = v^a \nabla_a t$ , and  $v^\phi = v^a \nabla_a \phi$  are invariant, while  $v^\theta = v^a \nabla_a \theta$  changes sign because  $\nabla_a \theta$  changes sign.

$$\Psi_l^m{}_\theta = \partial_\theta Y_l^m, \quad \Psi_l^m{}_\phi = \partial_\phi Y_l^m; \quad (40)$$

$$\Phi_l^m{}_\theta = -\frac{1}{\sin\theta} \partial_\phi Y_l^m, \quad \Phi_l^m{}_\phi = \sin\theta \partial_\theta Y_l^m; \quad (41)$$

$$\Phi_l^m{}_{\theta\theta} = Y_l^m, \quad \Phi_l^m{}_{\theta\phi} = 0; \quad (42)$$

$$\Phi_l^m{}_{\phi\phi} = \sin^2\theta Y_l^m; \quad (43)$$

$$\Psi_l^m{}_{\theta\theta} = \partial_\theta^2 Y_l^m, \quad \Psi_l^m{}_{\theta\phi} = (\partial_\theta \partial_\phi - \cot\theta \partial_\phi) Y_l^m, \quad (44)$$

$$\Psi_l^m{}_{\phi\phi} = (\partial_\phi^2 + \sin\theta \cos\theta \partial_\theta) Y_l^m; \quad (45)$$

$$\chi_l^m{}_{\theta\theta} = \frac{1}{\sin\theta} (\partial_\theta - \cot\theta) \partial_\phi Y_l^m, \quad \chi_l^m{}_{\theta\phi} = \frac{1}{2} \left( \frac{1}{\sin\theta} \partial_\phi^2 + \cos\theta \partial_\theta - \sin\theta \partial_\theta^2 \right) Y_l^m \quad (46)$$

$$\chi_l^m{}_{\phi\phi} = -\sin\theta (\partial_\theta - \cot\theta) \partial_\phi Y_l^m. \quad (47)$$

In Priou's (1992) notation (and with our own redefinitions mentioned in section 3), the perturbed metric  $h_{ab}$  is expressed in terms of ten  $\phi$ -dependent *perturbation functions*,  $h, p, k, w, q, a, b, L, M$ , and  $y$ , in the manner

$$h_{tt} = -2he^{2\nu} + (2y\omega + 2w\omega^2)e^{2\psi} \quad (48)$$

$$h_{tr} = L + a\omega e^{2\psi} \quad (49)$$

$$h_{t\theta} = M + b\omega e^{2\psi} \quad (50)$$

$$h_{t\phi} = -e^{2\psi}(y + 2\omega w) \quad (51)$$

$$h_{rr} = 2ke^{2\alpha} \quad (52)$$

$$h_{r\theta} = q \quad (53)$$

$$h_{r\phi} = -ae^{2\psi} \quad (54)$$

$$h_{\theta\theta} = 2pr^2 e^{2\alpha} \quad (55)$$

$$h_{\theta\phi} = -be^{2\psi} \quad (56)$$

$$h_{\phi\phi} = 2we^{2\psi}, \quad (57)$$

Equivalently, to first order in  $h_{ab}$

$$\begin{aligned}
 ds^2 &= -e^{2\nu}(1+2h)dt^2 + e^{2\psi}(1+2w)\left[d\phi - (\omega+y)dt - adr - bd\theta\right]^2 \\
 &+ e^{2\alpha}\left[(1+2k)dr^2 + r^2(1+2p)d\theta^2\right] \\
 &+ 2qdrd\theta + 2Ldtdr + 2Mdtd\theta.
 \end{aligned} \tag{58}$$

An associated set of real,  $\phi$ -independent, variables  $\hat{L}, \dots, \hat{w}$ , can be defined by writing

$$\hat{h} = he^{-im\phi}, \tag{59}$$

$$\hat{k} = ke^{-im\phi}, \tag{60}$$

$$\hat{L} = -iL e^{-im\phi}, \tag{61}$$

$$\hat{M} = -iM \sin\theta e^{-im\phi}, \tag{62}$$

$$\hat{q} = q \sin\theta e^{-im\phi}, \tag{63}$$

$$\hat{y} = y \sin^2\theta e^{-im\phi}, \tag{64}$$

$$\hat{a} = -ia \sin^2\theta e^{-im\phi}, \tag{65}$$

$$\hat{b} = -ib \sin^3\theta e^{-im\phi}, \tag{66}$$

$$\hat{p} = p \sin^2\theta e^{-im\phi}, \tag{67}$$

$$\hat{w} = w \sin^2\theta e^{-im\phi}. \tag{68}$$

Then, the metric perturbations of these modes can be expanded as follows in terms of Legendre polynomials:

$$\hat{h}, \hat{k}, \hat{L}, \hat{y}, \hat{a}, \hat{p}, \hat{w} \sim \sin^m\theta \sum_{\nu=0}^{\infty} a_{2\nu}(r) P_{2\nu}(\cos\theta), \tag{69}$$

$$\hat{M}, \hat{q}, \hat{b} \sim \sin^m \theta \sum_{l'=0}^{\infty} a_{2l'+1}(r) P_{2l'+1}(\cos \theta), \quad (70)$$

It is obvious from (69) and (70), that the functions  $\hat{M}, \hat{q}$  and  $\hat{b}$  will be antisymmetric about the equatorial plane, while all other functions will be symmetric. Furthermore, with these definitions, *the time-independent perturbed field equations become a system of ten real equations for ten real unknowns.*

The corresponding expansions for axial  $l = m$  modes, for which the tensor  $h_{ab}$  changes sign under reflection (modes that reduce to axial modes in the Regge-Wheeler gauge in the spherical limit), can easily be written in a similar fashion. We note that the behavior under reflection in the equatorial plane will be opposite to that of polar modes.

## 5. Gauge Choice

A linear perturbation of a star, described by the set of quantities  $(\delta\epsilon, \delta p, \delta u^a, h_{ab})$  is physically equivalent to the gauge-related perturbation described by the set  $(\delta\epsilon + \mathcal{L}_\eta\epsilon, \delta p + \mathcal{L}_\eta p, \delta u^a + \mathcal{L}_\eta u^a, h_{ab} + \mathcal{L}_\eta g_{ab})$  for any smooth vector field  $\eta^a$  that preserves the asymptotic behavior of the metric. The choice of gauge is important for the successful numerical solution of the perturbed field equations. After experimenting with a large number of possible gauges, we found that a numerical solution was more easily obtained in a gauge defined by the four conditions

$$h_{r\theta} = 0 \implies q = 0, \quad (71)$$

$$h_{\theta\phi} = 0 \implies b = 0, \quad (72)$$

$$h_{t\phi} = -\omega h_{\phi\phi} \implies y = 0, \quad (73)$$

$$h_{\phi\phi} = \frac{h_{\theta\theta}}{r^2} e^{2(\psi-\alpha)} \implies w = p. \quad (74)$$

The components of  $h_{ab}$  satisfy all imposed boundary conditions in this gauge. In addition, we required that it reduce to the Regge-Wheeler polar gauge in the non-rotating limit, in which only  $h_{tt}$ ,  $h_{rr}$ ,  $h_{\theta\theta}$  and  $h_{\phi\phi}$  are non-zero, with  $h_{\theta\theta}$  and  $h_{\phi\phi}$  satisfying the equivalent of (74) in a Schwarzschild metric (see previous section). With this choice of gauge there are six nonzero metric functions in the list (61)–(68), namely  $h$ ,  $p$ ,  $k$ ,  $\hat{L}$ ,  $\hat{M}$  and  $\hat{a}$ . They will be expressed in terms of the function  $\delta U$  by solving six components of the field equation  $\delta R_{ab} = 8\pi\delta(T_{ab} - \frac{1}{2}g_{ab}T)$ ,  $(tt)$ ,  $(rr)$ ,  $(\theta\theta)$ ,  $(tr)$ ,  $(t\theta)$  and  $(r\theta)$ . Note that condition (74) implies that the perturbation function  $p$  does not have to be redefined, as in (67), because it has the desired angular behavior

$$p \sim \sin^m \theta \sum_{l'=0}^{\infty} a_{2l'}(r) P_{2l'}(\cos \theta). \quad (75)$$

In Appendix A we list the necessary components of the perturbation in the Ricci tensor in this gauge.

## 6. Numerical Solution

The task of solving the coupled system of six differential equations is not trivial. In the gauge specified in section 5 the  $(tt)$  and  $(\theta\theta)$  equations are elliptic for  $h$  and  $p$  respectively. The  $(rr)$  equation is parabolic for  $k$  (it is missing a  $\partial^2 k / \partial r^2$  derivative). The  $(tr)$  and  $(r\phi)$  equations are second order ordinary differential equations (ODEs) for  $L$  and  $a$  in the angular direction, while the  $(t\theta)$  equation is a second order ODE for  $M$  in the radial direction. Each type of equation requires its own finite-difference scheme and boundary conditions. Still, we were able to solve all six equations simultaneously on a 2-dimensional finite grid.

In the radial direction, the grid coincides with that of the equilibrium configuration; that is, it consists of a number of grid-points, uniformly spaced in the coordinate  $s$ , which

ranges from  $s = 0$  ( $r = 0$ ) to  $s = 1$  ( $r = \infty$ ), the equator always being at  $s = 0.5$  (the coordinate  $s$  is defined by (11)). In the angular direction a different grid is used. Following Ipser & Lindblom (1990), the  $n$  angular grid-points are located at the angles  $\mu_i = \cos \theta_i$  which correspond to the zeros of the Legendre polynomial of order  $2n - 1$ :  $P_{2n-1}(\mu_i) = 0$ . *This has the advantage of using only a small number of angular grid-points to describe the star, which results in a smaller linear system of equations to be solved.* Since the perturbation functions are either symmetric or antisymmetric when reflected in the equatorial plane, one need only solve for  $0 < \theta \leq \pi/2$ , and the boundary conditions at  $\theta = \pi/2$  are incorporated in the expressions for the angular derivatives. A drawback of this method is that stars with stiff equations of state ( $N < 1.0$ ) are less accurately described than stars with soft EOSs ( $N > 1.0$ ), because the former have discontinuous derivatives of energy density and metric functions across the surface and this results in the appearance of Gibbs phenomena in the angular derivatives.

The above choice of angular grid-points allows us to use high-order formulae for the angular derivatives. In all six equations, all first and second order angular derivatives are approximated as

$$\frac{\partial}{\partial \mu} f^\pm(s_i, \mu_j) = \sum_{k=1}^n D_{jk}^\pm f^\pm(s_i, \mu_k), \quad (76)$$

and

$$\frac{\partial^2}{\partial \mu^2} f^\pm(s_i, \mu_j) = \sum_{k=1}^n H_{jk}^\pm f^\pm(s_i, \mu_k), \quad (77)$$

where  $f^\pm$  is a function which is either symmetric (+) or antisymmetric (–) under the transformation  $\theta \rightarrow \pi - \theta$ , i.e.  $f^\pm(s, -\mu) = \pm f^\pm(s, \mu)$ . The functions  $D_{jk}^\pm$  and  $H_{jk}^\pm$  are derived in Appendix B and are constructed specifically for functions that have the angular

behavior

$$f^+ = \sin^m \theta \sum_{l'=0}^{\infty} a_{2l'} P_{2l'}(\mu), \quad (78)$$

like  $h, k, p, \hat{L}$  and  $\hat{a}$ , and

$$f^- = \sin^m \theta \sum_{l'=0}^{\infty} a_{2l'+1} P_{2l'+1}(\mu), \quad (79)$$

like  $\hat{M}$ .

In all equations, except for the parabolic equation ( $rr$ ), the first and second order radial derivatives are approximated by the standard, second order accurate, central difference formulae

$$\frac{\partial}{\partial s} f_{i,j} = \frac{f_{i+1,j} - f_{i-1,j}}{2\Delta s}, \quad (80)$$

and

$$\frac{\partial^2}{\partial s^2} f_{i,j} = \frac{f_{i+1,j} - 2f_{i,j} + f_{i-1,j}}{\Delta s^2}, \quad (81)$$

where  $\Delta s$  is the distance between two radial grid-points. In the parabolic equation ( $rr$ ), we use an implicit solution scheme; that is, we use a first order accurate, backwards, first radial derivative for  $k$ ,

$$\frac{\partial}{\partial s} f_{i,j} = \frac{f_{i,j} - f_{i-1,j}}{\Delta s}, \quad (82)$$

while for the first order derivatives of other functions involved in the ( $rr$ ) equation we still use the second order accurate equation (80). Second order radial derivatives in the

( $rr$ ) equation are not approximated by (81) but by a similar equation using twice the grid-spacing

$$\frac{\partial^2}{\partial s^2} f_{i,j} = \frac{f_{i+2,j} - 2f_{i,j} + f_{i-2,j}}{(2\Delta s)^2}. \quad (83)$$

If one tries to use (81), the solution for  $k$  oscillates. That using (83) instead of (81) can suppress such oscillations was discovered in the construction of equilibrium models, where a second order radial derivative appears in the source term of a non-elliptic equation, by Stergioulas & Friedman (1995). Mixed derivatives involved in some of the equations are approximated by

$$\frac{\partial^2}{\partial s \partial \mu} f_{i,j}^{\pm} = \frac{1}{\Delta s} \sum_{k=1}^n D_{jk}^{\pm} (f_{i,k} - f_{i-1,k}). \quad (84)$$

At the center and at infinity the appropriate boundary finite difference formulae are used in all equations.

For the two elliptic equations ( $rr$ ) and ( $\theta\theta$ ) we require that the solution has vanishing first order angular derivative at  $\theta = \pi/2$  and vanishes at infinity. The boundary condition at  $\theta = \pi/2$  is built into the construction of the angular derivative formulae. No boundary conditions are needed at the center and on the symmetry axis for the elliptic equations, but the discretized equations force the solution to vanish there for any mode with  $m \neq 0$ , as is the case for the exact solution.

For the two second order angular ODE's, ( $tr$ ) and ( $r\phi$ ), the boundary conditions at  $\theta = \pi/2$  and on the symmetry axis are set by the angular derivative equations (76) and (77). For the second order radial ODE ( $t\theta$ ) we require that  $\hat{M}$  vanishes at the center and at infinity. Finally, for the parabolic equation ( $rr$ ), boundary conditions at  $\theta = \pi/2$  and on the symmetry axis are set by the angular derivative equations (76) and (77), while in the

radial direction we set  $k = 0$  at the center only (at infinity the boundary is open).

Of the above equations, the most difficult to solve numerically are the  $(rr)$  and  $(r\phi)$  equations. In the  $(rr)$  equation, the solution is propagated from the center to infinity via a first order radial derivative, so it is far more sensitive to local inaccuracies (like those produced by the finite grid-spacing at the surface) than the elliptic equations. In particular, the surface of the rotating star does not correspond to a constant value of the radial coordinate but falls in between grid points. For polytropes of index  $N \geq 2$ , the energy density goes smoothly enough to zero at the surface that this does not pose any problem even with a grid of only 200 radial points. For polytropes of index  $1 \leq N < 2$ , however, a small jump in the solution for  $k$  appears at the surface. Stiff polytropes of index  $N < 1$  have, in addition, discontinuous second order derivatives of the equilibrium metric functions across the surface and a jump in the numerical solution for  $k$  is unavoidable when using our grid, since the angular derivative equations were designed only for smooth functions. The small jump appearing in the numerical solution for  $k$  does not affect any other perturbation function significantly, except for the function  $a$ . Another problem with the  $(rr)$  equation - of same origin - is that, for stiff equations of state, the solution oscillates in the vacuum region, unless one makes the approximation

$$\frac{\partial^2 h}{\partial s^2} + 2 \frac{\partial^2 p}{\partial s^2} \simeq - \frac{\partial^2 h}{\partial s^2}. \quad (85)$$

The error introduced by making this approximation is small, since for all stars that we examined

$$h \simeq -p. \quad (86)$$

Thus, the significant benefit of making this approximation (suppression of all oscillations in

the solution) outweighs its mild cost.

Finally, the  $(r\phi)$  equation seems to be very sensitive to local inaccuracies, especially at the surface of the star and near its center. The inaccuracies near the center of the star occur, because the perturbation function  $a$  depends on the *differences* between other perturbation functions, which all have very small values (compared to their maximum value) near the center. However, the perturbation function  $a$  is of lesser importance compared to the other five functions, when computing the critical angular velocities. In fact, we determined that  $a$  only minimally affects the other five perturbation functions, so that setting it equal to zero, results in almost unchanged solutions for the other perturbation functions and unchanged critical angular velocities for even the most relativistic stars of the stiffest polytropic index ( $N = 1.0$ ) we examined.

We also determined that the other two off-diagonal perturbation functions  $\hat{L}$  and  $\hat{M}$  are weakly coupled to the diagonal ones. This is expected, since in our gauge the perturbed metric reduces to a diagonal form in the non-rotating limit and  $h_{t\phi}$  is the dominant off-diagonal perturbation ( $g_{t\phi}$  is the only non-vanishing off-diagonal metric element for a rotating star). We emphasize that all the above statements hold for perturbations *of the type considered in the present paper*.

The finite-differencing of the system of perturbed field equations yields a large linear system. The unknowns are ordered in a way that casts the matrix of the linear system in a band-diagonal form. A direct solution method (LU-decomposition) is employed. Alternatively, we also use an iterative Bi-Conjugate Gradient method with a *symmetric successive over-relaxation (SSOR) method* as a preconditioner. The direct solution was faster, but required a larger amount of random access memory.<sup>3</sup>

---

<sup>3</sup>The subroutines for the solution of the linear system we used, are part of the Portable

A representative solution of the coupled system of six perturbation equations, for a specific trial function  $\delta U$ , is shown in Figs. (1) - (3). The background star is a rapidly rotating,  $N=1.5$  polytrope with dimensionless central energy density  $\bar{\epsilon}_c = 0.061$  and dimensionless angular velocity  $\bar{\Omega} = 0.092$ . The solution was obtained for the  $l = m = 3$  mode using a trial function

$$\delta U = r^l P_l^m(\mu), \tag{87}$$

where  $P_l^m(\mu)$  is the associated Legendre function. This trial function is the dominant term in the true eigenfunction of the  $l = m$  modes (see section 8). All six equations were solved on the same  $101 \times 7$  (radial  $\times$  angular) grid. The perturbation functions  $h, p, k, \hat{L}, \hat{M}$  and  $\hat{a}$  are shown along all seven angular spokes and at the pole (where they vanish). With the exception of  $\hat{M}$ , the perturbation functions are symmetric under reflection in the equatorial plane and their maximum value occurs for  $\theta = \pi/2$ . The perturbation function  $\hat{M}$  is antisymmetric under reflection, so it vanishes at  $\theta = \pi/2$ . Its maximum value occurs about half-way between the pole and the equator. The diagonal perturbation functions  $h, p$  and  $k$  have no nodes inside the star. This is a characteristic of  $h_{tt}$  for fundamental  $l = m$  modes in the Newtonian limit. The perturbation function  $k$  (the solution to the parabolic ( $rr$ ) equation) exhibits a small jump at the surface, as was explained earlier. In addition, near the surface, the solution can have a wave-like character. This is normal and arises because the solution is obtained for a trial function  $\delta U$  and *not* for the true eigenfunction. The off-diagonal functions  $\hat{L}, \hat{M}$  and  $\hat{a}$  vanish much faster in the vacuum surrounding the star than the diagonal functions do; they become negligible almost immediately outside the surface of the star. The function  $\hat{L}$  does not have any node inside the star, but  $\hat{M}$  and  $\hat{a}$

---

Extensible Toolkit for Scientific Computation (PETSc) package developed at Argonne National Laboratory (Gropp and Smith 1994) .

do. Finally, the solution for the function  $\hat{a}$  exhibits some oscillations at the surface of the star, which are induced by the behavior of the function  $k$  there. Regarding other polytropic indices and modes, the perturbation functions remain similar to those in Figs. (1) - (3). For stiffer polytropes and for more relativistic stars, the solutions are peaked closer to the surface than for softer polytropes and less relativistic stars. For larger  $m$ , the solutions are more narrowly peaked about their maximum value because the dominant radial behavior of  $\delta U$  is  $r^l$ . For  $N = 1.0$  polytropes the oscillations at the surface are larger than for  $N = 1.5$  polytropes, while for  $N = 2.0$  polytropes they are negligible. Otherwise, the solutions for the perturbation functions are very similar to those in Figs. (1) - (3).

## 7. A Truncated Gauge

In the Newtonian limit, the important component of the perturbation  $h_{ab}$  is  $h_{tt}$ , which reduces to  $-2h$ . In addition, the metric functions  $h$ ,  $k$ ,  $p$  and  $w$  satisfy the relation

$$h = -k = -p = -w. \tag{88}$$

For energy densities typical in neutron stars, the  $h_{tt}$  component still dominates  $h_{ab}$ . We determined numerically, that even for the most relativistic and rapidly rotating  $N = 1.0$  polytrope, the relation (88) still holds approximately in our gauge. This led us to investigate whether by making certain approximations, one can still obtain accurate values for the critical angular velocities of neutral modes, while solving fewer than six equations. Indeed, we find that by making the approximations

$$\frac{h_{tt}}{g_{tt} + 2\omega g_{t\phi}} = \frac{h_{rr}}{g_{rr}} = \frac{h_{\theta\theta}}{g_{\theta\theta}} \implies h = -k = -p, \tag{89}$$

and

$$h_{t\theta} = h_{r\phi} = 0 \quad \implies \quad \hat{M} = \hat{a} = 0, \quad (90)$$

one can obtain very accurate critical angular velocities, while solving only two perturbed field equations. Equation (89) is motivated by (88) and (90) is used since  $g_{t\theta} = g_{t\phi} = 0$  for the equilibrium configuration and because  $h_{t\theta}$ ,  $h_{r\phi}$  vanish in the spherical limit in the Regge-Wheeler polar gauge, i.e. they are proportional to the background metric function  $\omega$ . In this *truncated gauge*, the perturbation in the metric tensor, can be written in the form

$$h_{ij} = \begin{pmatrix} -2h(e^{2\nu} - \omega^2 e^{2\psi}) & L & 0 & -2\omega h e^{2\psi} \\ & -2h e^{2\alpha} & 0 & 0 \\ \text{sym.} & & -2hr^2 e^{2\alpha} & 0 \\ & & & -2h e^{2\psi} \end{pmatrix}. \quad (91)$$

Only two perturbation functions are nonzero,  $h$  and  $\hat{L}$ , which are determined by solving the  $(tt)$  and  $(tr)$  equations.

Table 1 shows a comparison of critical configurations obtained in the full and truncated gauges. The equilibrium star is a  $N = 1.0$  polytrope with  $\bar{\epsilon}_c = 0.3$ , which is close to the central energy density of the maximum mass configuration. The critical configurations for the  $l = m = 3, 4$  and 5 modes are computed in both gauges on the same  $101 \times 7$  grid. We compare the dimensionless critical angular velocity and the critical ratio of rotational to gravitational binding energy  $T/|W|_c$  in the two gauges. The critical values of  $T/|W|$  differ by less than 1% and the critical angular velocities by less than 0.5% when computed in the truncated gauge compared to computing them in the full gauge. The advantage of using the truncated gauge is that far less memory is needed by the numerical code. While six equations can be solved in a reasonable time with a maximum  $201 \times 12$  grid on a DEC Alpha with 256 MBytes of memory, two equations can be solved with a much

finer grid of  $801 \times 12$  or more points. The execution speed is not limited by the processor speed (the matrix inversion is very fast) but by the available random access memory. For very soft polytropes of index  $N \geq 2.0$ , a  $201 \times 12$  grid gives sufficiently accurate critical angular velocities, so that one can use the full gauge for these models. But, for polytropes of  $N \leq 1.0$  a  $201 \times 12$  grid determines the critical angular velocity with an error that can exceed several percent or more. This was determined by comparing critical configurations for Newtonian polytropes, obtained with our code, to published results. Thus, for realistic neutron stars, it is necessary to obtain the critical angular velocities with a grid of at least  $801 \times 12$  points and this could be achieved only in the truncated gauge. For this reason, *all results reported in the present paper* were obtained in the truncated gauge with a grid of  $801 \times 12$  points, unless otherwise stated.

## 8. The Perturbed Energy Conservation Equation

In preceding sections it was shown how a solution of the perturbed field equations is obtained for a given trial function  $\delta U$ . The complete description of the neutral modes requires the satisfaction of both the perturbed field equations (16) and the perturbed energy conservation equation (34) by the perturbation in the metric  $h_{ab}$  and the scalar function  $\delta U$ . This system of equations (16) and (34) has a zero-frequency solution only for the stars for which a zero-frequency mode exists. For any equilibrium model, however, one can solve only the perturbed field equations (16) for trial functions  $\delta U$  and use the perturbed energy conservation equation (34) to construct a criterion for locating the marginally stable star (for a given mode) along a sequence of rotating stars.

The perturbed field equations (16) are implicitly linear in the function  $\delta U$ , as is the perturbed energy conservation equation (34). Hence (34) can be represented as a linear operator  $L$  acting on a function  $\delta U$

$$L(\delta U) = 0. \tag{92}$$

Equation (92) represents an eigenvalue problem for the linear operator  $L$  with zero eigenvalue and eigenfunction  $\delta U$ .

In the Newtonian limit, it was shown that the eigenfunction  $\delta U$  of an  $l = m$  neutral mode can be approximated accurately by expanding it in terms of a set of basis functions  $\delta U_i$ ,

$$\delta U = \sum_i a_i \delta U_i, \tag{93}$$

of the form

$$\delta U_i = \delta U_i^{(jk)} = r^{l+2(j+k)} Y_{l+2k}^m(\cos \theta), \tag{94}$$

with  $j, k = 0, 1, \dots$  and with each set of indices  $(j, k)$  yielding a particular  $\delta U_i$ . In practice the eigenfunction  $\delta U$  is represented with reasonable accuracy by only a few terms, and the  $(0, 0)$  term  $r^l Y_l^m$  dominates the expansion (94).

Substituting the expansion (93) in (92) yields

$$\sum_i a_i L(\delta U_i) = 0. \tag{95}$$

If we define the inner product<sup>4</sup>

---

<sup>4</sup>The motivation for defining the inner product as in (96) will become apparent in Appendix C.

$$\langle \delta U_j | L | \delta U_i \rangle = \int i \frac{\delta U_j}{\sigma u^t} L(\delta U_i) \sqrt{-g} d^3 x, \quad (96)$$

where  $g$  is the determinant of the equilibrium metric tensor, then taking the inner product of (95) with respect to  $\delta U_j$  yields

$$\sum_i a_i \langle \delta U_j | L | \delta U_i \rangle = 0. \quad (97)$$

Although the basis functions are not orthogonal to each other, non-zero  $\langle \delta U_j | \delta U_i \rangle$  terms do not appear on the r.h.s. of (97) because we require that the eigensystem has zero eigenvalue. The last equation is a linear, homogeneous system for the coefficients  $a_i$ . The system has a non-trivial solution only if its determinant vanishes. This yields a criterion for locating the zero-frequency modes

**Criterion** *A stationary, axisymmetric model has a nonaxisymmetric, zero-frequency mode with angular dependence  $e^{im\phi}$ , if*

$$\det \langle \delta U_j | L | \delta U_i \rangle = 0. \quad (98)$$

In practice, we start with a slowly rotating star and compute the matrix elements  $\langle \delta U_j | L | \delta U_i \rangle$ . For slowly rotating stars the determinant in (98) always has a large value. Keeping the central energy density constant, we look at stars of increasing angular velocity, until the determinant goes through zero. The star for which (98) is satisfied is the one for which the particular  $l = m$  mode has a zero-frequency solution and the nonaxisymmetric instability sets in through that mode. In this method, the accuracy in locating the neutral modes depends on how well the expansion (93) approximates the true eigenfunction  $\delta U$ .

In Appendix C, we obtain, in terms of Eulerian quantities, an expression for  $\langle \delta U_j | L | \delta U_i \rangle$  that is used in the numerical computations. As discussed in this Appendix the above method of solving the perturbed energy conservation equation is not identical to using a variational principle; because of our choice of field equations, the matrix  $\langle \delta U_j | L | \delta U_i \rangle$  is not symmetric. For central energy densities typical in neutron stars, however, the matrix is nearly symmetric and the method nearly coincides with a variational principle.

## 9. Critical configurations

Following the method developed in previous sections, we computed the neutral mode (critical) configurations for the fundamental  $l = m = 2, 3, 4$  and  $5$  nonaxisymmetric modes. Three equations of state were examined, having polytropic indices  $N = 1.0, 1.5$  and  $2.0$  polytropes. The  $N = 1.0$  polytropes include models with mass and radius similar to those of realistic neutron stars. The other two equations of state were examined for completeness and for comparison with published results in the Newtonian limit. The critical configurations were computed in the truncated gauge with a fine grid of up to  $801 \times 12$  (radial  $\times$  angular) grid points. The trial function  $\delta U$  was expanded as in (94) using different number of terms. Eight basis functions, corresponding to the indices  $j = 0, \dots, 3$  and  $k = 0, 1$  in (94) were sufficient to determine the critical configurations with good accuracy, especially for the  $N = 1.5$  and  $N = 2.0$  polytropes, where the error consistently decreases with increasing number of basis functions and increasing number of grid points. This was not so for the  $N = 1.0$  polytropes. Owing to the finite grid-size, the surface of the star is discontinuous, and this gives rise to Gibbs phenomena at the surface when using the expansions (76), (77) for the angular derivatives. As a result, increasing the number of grid-points did not monotonically decrease the error. This behavior is expected for our choice of coordinates

and grid. It is the price one has to pay for being able to solve a smaller than otherwise linear system of equations. A similar behavior is reported in Bonazzola *et al.* (1996), who use a similar angular grid in computing the neutral, viscous bar mode in relativistic stars. Still, by computing the  $N = 1.0$  configurations with various grid sizes and various numbers of basis functions, we could obtain sufficiently accurate results.

Our code was checked in the Newtonian limit by comparing the critical configurations for the  $l = m = 3, 4$  and  $5$  modes for  $N = 1.0, 1.5$  and  $2.0$  polytropes to results published by Managan (1985), Imamura, Friedman & Durisen (1985) and Ipser & Lindblom (1990). As can be seen in Table 2 we are in very good agreement with all published Newtonian results, the exception being  $T/|W|_c$  for the  $m = 5$  mode in  $N = 1.0$  polytropes, which differs by 2 % from the value published in Ipser & Lindblom (1990), from which Imamura, Friedman & Durisen (1985) differ by 3 % (in the opposite direction). This highlights the increased inaccuracy involved in computing neutral modes for  $N \leq 1.0$  polytropes.

For relativistic polytropes we obtain the following results: For  $N = 1.0$ , figure 4 shows the ratio of the critical angular velocity  $\Omega_c$  to the *Keplerian angular velocity*  $\Omega_K$  at same central energy density as a function of central energy density for the four modes examined. The lowest central energy density in the figure corresponds to a mildly relativistic star. The highest central energy density shown is the central energy density of the most massive (and thus most relativistic) star allowed by the particular equation of state. The filled circles on the left vertical axes represent the values of  $\Omega_c/\Omega_K$  in the Newtonian limit. As the central energy density increases and the star becomes more relativistic,  $\Omega_c/\Omega_K$  decreases and it decreases at a faster rate as it approaches the most relativistic configuration. Contrary to the Newtonian limit, where  $N = 1.0$  polytropes do not have an unstable  $m = 2$  mode, we find that in relativistic  $N = 1.0$  polytropes the  $m = 2$  mode becomes unstable when the central energy density exceeds roughly one 10th the central energy density of the most

massive star. At the most relativistic configuration, the  $m = 2$  mode becomes unstable for  $T/|W|_c=0.065$  or  $\Omega_c/\Omega_K = 0.91$ . Table 4 compares the most relativistic critical configurations to their counterparts in the Newtonian limit. The value of  $\Omega_c/\Omega_K$  decreases by roughly 15% for the  $m = 3, 4$  and 5 modes. Figure (5) shows the critical ratio  $T/|W|_c$  for the same  $N = 1.0$  polytropes. This ratio decreases faster and by a larger percentage than  $\Omega_c/\Omega_K$ , owing to the fact that the Keplerian value  $T/|W|_K$  also decreases as one samples more relativistic stars. In Table 3 it is shown that for the most relativistic  $N = 1.0$  polytrope the critical ratio  $T/|W|_c$  is about 40 % smaller, for the  $m = 3, 4$  and 5 modes, than the corresponding ratio in the Newtonian limit. When the decrease in the Keplerian value  $T/|W|_K$  is taken into account and one looks at the ratio  $(T/|W|_c)/(T/|W|_K)$  the most relativistic values are still 25 – 30% lower than the Newtonian values.

Figures (6) and (7) and Table 4 display the critical configurations for  $N = 1.5$  polytropes. These polytropes are softer than the ones with index  $N = 1.0$ . Consequently, they have a smaller maximum mass and are less relativistic. For this reason, relativity has a smaller effect on the onset of the nonaxisymmetric instability. The  $m = 2$  mode does not become unstable even for the most relativistic  $N = 1.5$  polytropes. For the  $m = 3, 4$  and 5 modes, the value of  $\Omega_c/\Omega_K$  decreases by 7 – 10% for the most relativistic models compared to the Newtonian limit. The corresponding decrease for  $T/|W|_c$  is 30 – 35% and for  $(T/|W|_c)/(T/|W|_K)$  it is 13 – 19%.

Plots of  $\Omega_c/\Omega_K$  and  $T/|W|_c$  for the  $N = 2.0$  polytropes are shown in figures (8) and (9). These are extremely soft models and their maximum mass occurs at nearly Newtonian central energy densities. Again, the  $m = 2$  mode does not become unstable. As seen in table 5, for the  $m = 3, 4$  and 5 modes the values of  $\Omega_c/\Omega_K$ ,  $T/|W|_c$  and  $(T/|W|_c)/(T/|W|_K)$  are only a few percent less than in the Newtonian limit, for the largest central energy density. Polytropes constructed with  $N = 2.0$  do not resemble realistic neutron stars, but

are included here for completeness.

Regarding the accuracy of our results, we estimate that the determined critical angular velocities and critical  $T/|W|_c$  are accurate to better than 2 % for  $N = 1.0$ , 1-2 % for  $N = 1.5$  and 1 % for  $N = 2.0$  polytropes.

## 10. Discussion

We have treated nonaxisymmetric neutral modes in the context of general relativity. We have found a gauge in which six coupled perturbed field equations can be solved simultaneously with good accuracy. Furthermore, we found an approximate gauge, in which the critical configurations for  $N \geq 1.0$  polytropes are located with sufficient accuracy, while solving only two independent perturbed field equations. We showed that general relativity has a large effect on the location of nonaxisymmetric neutral modes and forces the nonaxisymmetric instability to set in for smaller rotation rates than Newtonian theory suggests.

The large effect of relativity on the onset of the nonaxisymmetric instability is most striking in the case of the  $m = 2$  modes. In the Newtonian context it was shown that uniformly or nearly uniformly rotating neutron stars cannot become unstable to the  $m = 2$  mode unless the equation of state is excessively stiff (see e.g. Skinner & Lindblom (1996) ). For polytropes, the classical result by James (1964) restricts the onset of the  $m=2$  instability to polytropes having an adiabatic index larger than  $\Gamma_{\text{crit}} = 2.237$  (which corresponds to a polytropic index  $N_{\text{crit}} = 0.808$ ). We find that, in the context of general relativity, this critical value becomes  $\Gamma_{\text{crit}} = 1.77$  (polytropic index  $N_{\text{crit}} = 1.3$ ).

In the Newtonian limit, the  $m = 2$  mode driven by gravitational radiation coincides with the  $m=2$  mode driven by viscosity even for compressible fluids, as was shown by Ipser

& Managan (1985) . It is interesting that work by Bonazzola *et al.* (1996) suggests that in general relativity, the  $m = 2$  viscosity-driven mode has a critical adiabatic index only *slightly higher* than James’s result. Thus, in general relativity, the viscosity driven and the gravitational radiation driven  $m = 2$  modes no longer coincide and the effect of relativity seems to be very different on each of them.

In forthcoming work, we plan to study realistic equations of state and include the effect of viscosity on the onset of the nonaxisymmetric instability.

We would like to thank Lee Lindblom, Jim Ipser, Yoshiharu Eriguchi and Ed Seidel for very helpful discussions. This research has been supported by NSF grants PHY-9105935 and PHY-9507740.

## A. Perturbed Ricci Tensor

We list the perturbation in the six components of the Ricci tensor that are used in the perturbed field equations, in the gauge of section 5. We follow the notation introduced in section 4. In the r.h.s. of each equation, subscripts denote partial derivatives, e.g.  $h_{\phi\phi} = \partial^2 h / \partial \phi^2$ .

$$\begin{aligned}
 \delta R_{tt} = & -\omega^2(h_{\phi\phi} + p_{\phi\phi}) + e^{2(\nu-\psi)}h_{\phi\phi} + e^{2(\psi-\nu)}\omega^4 p_{\phi\phi} + e^{2(\nu-\alpha)} \left\{ 2\nu_{rr}(h - k) \right. \\
 & + 2\nu_r(h_r - k_r) + 2\left(\nu_r + \frac{1}{r}\right)\nu_r(h - k) + \frac{2}{r^2}[\nu_{\theta\theta}(h - p) + \nu_\theta(h_\theta - p_\theta) \\
 & + \nu_\theta^2(h - p)] + \nu_r[a_\phi + 2\psi_r(h - k) + k_r + 2p_r] + \frac{\nu_\theta}{r^2}[2\psi_\theta(h - p) \\
 & + k_\theta + 2p_\theta] + h_{rr} + \frac{h_{\theta\theta}}{r^2} + \left(\psi_r + \frac{1}{r}\right)h_r + \frac{\psi_\theta}{r^2}h_\theta \left. \right\} \\
 & + e^{2(\psi-\alpha)} \left\{ -\omega^2\left(p_{rr} + \frac{p_{\theta\theta}}{r^2}\right) + \omega\psi_r[2\omega\psi_r(p - k) + \omega a_\phi - \omega(h_r + k_r) \right.
 \end{aligned}$$

$$\begin{aligned}
& + p_r] - \frac{\omega^2}{r^2} \psi_\theta (h_\theta + k_\theta + p_\theta) + \omega [2\omega_r \psi_r (k - p) + 2\omega \psi_{rr} (k - p) \\
& + 2\omega \psi_r (k_r - p_r)] + 2\omega^2 \left( \nu_r + \frac{1}{r} + 2\psi_r \right) \psi_r (k - p) - \omega^2 \nu_r (2a_\phi + p_r) \\
& - \frac{\omega^2}{r^2} \nu_\theta p_\theta - \frac{\omega^2}{r} p_r \left. \vphantom{\frac{\omega^2}{r^2} \nu_\theta p_\theta} \right\} - \omega^2 e^{2(\psi - \alpha - \nu)} \left[ \psi_r \omega L_\phi + \frac{\psi_\theta}{r^2} \omega M_\phi \right] \\
& + e^{-2\alpha} \left\{ L_\phi [\omega_r + \omega(2\psi_r - \nu_r)] + \frac{M_\phi}{r^2} [\omega_\theta + \omega(2\psi_\theta - \nu_\theta)] \right\} \\
& + e^{4\psi - 2(\alpha + \nu)} \left[ \omega^3 \omega_r a_\phi + \omega^2 \omega_r^2 (h + k - 2p) + \frac{1}{r^2} \omega^2 \omega_\theta^2 (h - p) \right] \\
& + e^{2(\psi - \alpha)} \left\{ (k - p) \left[ \omega_r^2 + \omega \omega_r \left( 4\psi_r - 2\nu_r + \frac{2}{r} \right) + 2\omega \omega_{rr} \right] \right. \\
& \left. + \omega_r \omega (h_r + k_r - 4p_r) + \frac{\omega_\theta}{r^2} \omega (h_\theta - 2p_\theta - k_\theta) \right\} \tag{A1}
\end{aligned}$$

$$\begin{aligned}
\delta R_{rr} = & \left( -e^{2(\alpha - \psi)} + \omega^2 e^{2(\alpha - \nu)} \right) k_{\phi\phi} - \frac{k_{\theta\theta}}{r^2} - h_{rr} - 2p_{rr} - a_{r\phi} - \frac{k_\theta}{r^2} (\nu_\theta + \psi_\theta) \\
& + k_r \left( \nu_r + \frac{1}{r} + \psi_r \right) + \frac{2}{r^2} [\alpha_{\theta\theta} (p - k) + \alpha_\theta (p_\theta - k_\theta) \\
& + \alpha_\theta (\nu_\theta + \psi_\theta) (p - k)] - \frac{\alpha_\theta}{r^2} (h_\theta + 2p_\theta - k_\theta) + \alpha_r (h_r + k_r + a_\phi) \\
& - 2\psi_r (p_r + a_\phi) - 2\nu_r h_r - \frac{2}{r} p_r + \omega e^{-2\nu} \left( -\frac{\alpha_\theta}{r^2} M_\phi + \alpha_r L_\phi - L_{r\phi} \right) \\
& + \omega_r e^{2(\psi - \nu)} [-\omega a_\phi + \omega_r (p - h)] \tag{A2}
\end{aligned}$$

$$\begin{aligned}
\delta R_{\theta\theta} = & \left( -e^{2(\alpha - \psi)} + \omega^2 e^{2(\alpha - \nu)} \right) r^2 p_{\phi\phi} - r^2 p_{rr} - h_{\theta\theta} - k_{\theta\theta} - p_{\theta\theta} - r^2 p_r \left( \nu_r + \frac{1}{r} \right. \\
& \left. + \psi_r \right) + p_\theta (\nu_\theta + \psi_\theta) + 4r \left( \alpha_r + \frac{1}{r} \right) (k - p) + 2r^2 \left( \alpha_{rr} - \frac{1}{r^2} \right) (k - p) \\
& + 2r^2 \left( \alpha_r + \frac{1}{r} \right) (k_r - p_r) + 2 \left( \nu_r - \frac{1}{r} + \psi_r \right) r^2 \left( \alpha_r + \frac{1}{r} \right) (k - p) \\
& - r^2 \left( \alpha_r + \frac{1}{r} \right) (h_r + k_r + a_\phi) + \alpha_\theta (h_\theta + 2p_\theta - k_\theta) - 2\psi_\theta p_\theta - 2\nu_\theta h_\theta \\
& + \omega e^{-2\nu} \left[ -r^2 \left( \alpha_r + \frac{1}{r} \right) L_\phi + \alpha_\theta M_\phi - M_{\theta\phi} \right] + \omega_\theta^2 e^{2(\psi - \nu)} (p - h) \tag{A3}
\end{aligned}$$

$$\begin{aligned}
\delta R_{tr} = & -\frac{\omega}{2}a_{\phi\phi} + \omega(h_{r\phi} - p_{r\phi}) + \omega(2p_{\phi} + h_{\phi} - k_{\phi})(\nu_r - \psi_r) + \frac{\omega^3}{2}e^{2(\psi-\nu)}a_{\phi\phi} \\
& + \frac{1}{2}e^{2(\psi-\alpha)}\left\{-2a\omega\psi_r\left(\nu_r + \frac{1}{r} + \psi_r\right) + \frac{\omega}{r^2}\psi_{\theta}(-3a_{\theta} - 2a\psi_{\theta} - 2a\nu_{\theta})\right. \\
& + \frac{\omega}{r^2}(2\alpha_{\theta} - \nu_{\theta})a_{\theta} - \frac{\omega}{r^2}a_{\theta\theta} - 2a\omega\left(\psi_{rr} + \frac{\psi_{\theta\theta}}{r^2}\right)\left.\right\} + \frac{1}{2}(-e^{-2\psi} + \omega^2e^{-2\nu})L_{\phi\phi} \\
& + \frac{\omega_r}{2}(k_{\phi} - h_{\phi} - 2p_{\phi}) - \frac{1}{2}a\omega e^{4\psi-2(\alpha+\nu)}\left(\omega_r^2 + \frac{\omega_{\theta}^2}{r^2}\right) + \frac{\omega^2}{2}\omega_r e^{2(\psi-\nu)}(h_{\phi} + k_{\phi} \\
& - 4p_{\phi}) + \frac{1}{2}e^{2(\psi-\alpha)}\left\{a\omega_r\left(\nu_r - 3\psi_r - \frac{1}{r}\right) + \frac{a}{r^2}\omega_{\theta}(\nu_{\theta} - 3\psi_{\theta}) - a\left(\psi_{rr} + \frac{\psi_{\theta\theta}}{r^2}\right)\right. \\
& - \left.\frac{\omega_{\theta}}{r^2}a_{\theta}\right\} + \frac{1}{2}e^{2(\psi-\alpha-\nu)}\left\{\omega\omega_r\left[L\left(3\psi_r - \nu_r + \frac{1}{r}\right) + \frac{M}{r^2}(3\psi_{\theta} - 2\alpha_{\theta} - \nu_{\theta})\right.\right. \\
& + \left.\left.\frac{M_{\theta}}{r^2}\right] + \frac{\omega}{r^2}\omega_{\theta}(2L\alpha_{\theta} - L_{\theta}) + \frac{\omega_r}{r^2}\omega_{\theta}M + \omega_r^2L + \frac{1}{r^2}\omega\omega_{r\theta}M + \omega\omega_{rr}L\right\} \\
& + e^{-2\alpha}\left\{-L\left(\frac{2}{r^2}\alpha_{\theta}\nu_{\theta} + \frac{1}{r}\nu_r + \nu_r^2 + \nu_r\psi_r + \nu_{rr}\right) + \frac{M}{r^2}(2\alpha_{\theta}\nu_r - \nu_r\nu_{\theta}\right. \\
& - \left.\nu_r\psi_{\theta} - \nu_{r\theta}) + \frac{M_r}{r^2}\left(\frac{\psi_{\theta}}{2} + \frac{\nu_{\theta}}{2} - \alpha_{\theta}\right) + \frac{L_{\theta}}{r^2}\left(-\frac{\psi_{\theta}}{2} + \frac{\nu_{\theta}}{2} + \alpha_{\theta}\right) - \frac{\nu_r}{r^2}M_{\theta}\right. \\
& \left. - \frac{L_{\theta\theta}}{2r^2} + \frac{M_{r\theta}}{2r^2}\right\} \tag{A4}
\end{aligned}$$

$$\begin{aligned}
\delta R_{t\theta} = & \omega(h_{\theta\phi} - p_{\theta\phi}) + (\nu_{\theta} - \psi_{\theta})\omega(k_{\phi} + h_{\phi}) + \frac{1}{2}e^{2(\psi-\alpha)}\left[3\omega\psi_r a_{\theta} - \omega\left(2\alpha_r + \frac{1}{r}\right.\right. \\
& \left.\left.- \nu_r\right)a_{\theta} + \omega a_{r\theta}\right] + \frac{1}{2}(-e^{-2\psi} + \omega^2e^{-2\nu})M_{\phi\phi} - \frac{\omega_{\theta}}{2}(h_{\phi} + k_{\phi}) \\
& + \frac{\omega^2}{2}\omega_{\theta}e^{2(\psi-\nu)}(h_{\phi} - 2p_{\phi} - k_{\phi}) + \frac{1}{2}e^{2(\psi-\alpha)}\omega_r a_{\theta} \\
& + \frac{1}{2}e^{2(\psi-\alpha-\nu)}\left\{\omega\omega_{\theta}\left[L(3\psi_r - 2\alpha_r - \nu_r - \frac{1}{r}) + \frac{M}{r^2}(3\psi_{\theta} - \nu_{\theta}) + L_r\right]\right. \\
& + \left.\omega\omega_r\left[2M\left(\alpha_r + \frac{1}{r}\right) - M_r\right] + L\omega_r\omega_{\theta} + L\omega\omega_{r\theta} + \frac{M}{r^2}(\omega_{\theta}^2 + \omega\omega_{\theta\theta})\right\} \\
& + e^{-2\alpha}\left\{-\frac{M}{r^2}\left[2r^2\nu_r\left(\alpha_r + \frac{1}{r}\right) + \nu_{\theta}^2 + \nu_{\theta}\psi_{\theta} + \nu_{\theta\theta}\right] + L\left[\left(2\alpha_r + \frac{1}{r}\right)\nu_{\theta}\right.\right. \\
& \left.\left.- \nu_r\nu_{\theta} - \nu_{\theta}\psi_r - \nu_{r\theta}\right] + \left(\frac{\psi_r}{2} + \frac{\nu_r}{2} - \alpha_r + \frac{1}{2r}\right)(L_{\theta} - M_r) - L_r\nu_{\theta}\right\}
\end{aligned}$$

$$+ \left. \frac{L_{r\theta}}{2} - \frac{M_{rr}}{2} \right\} \quad (\text{A5})$$

$$\begin{aligned} \delta R_{r\phi} = & -h_{r\phi} - p_{r\phi} + \psi_r(h_\phi + p_\phi) + \nu_r(k_\phi - h_\phi) + \left(\alpha_r + \frac{1}{r}\right)(k_\phi - p_\phi) \\ & - \frac{1}{2}e^{2(\psi-\nu)}\omega^2 a_{\phi\phi} + e^{2(\psi-\alpha)} \left\{ \frac{1}{2r^2} [2a_\theta\psi_\theta + 2a\psi_{\theta\theta} + a_{\theta\theta} + \nu_\theta(2a\psi_\theta + a_\theta)] \right. \\ & + a\psi_{rr} - \frac{\alpha_\theta}{r^2}a_\theta + a\psi_r\left(\nu_r + \frac{1}{r} + \psi_r\right) + \frac{\psi_\theta}{2r^2}(2a\psi_\theta + a_\theta) \left. \right\} - \frac{\omega}{2}e^{-2\nu}L_{\phi\phi} \\ & + \frac{a}{2}e^{4\psi-2(\alpha+\nu)}\left(\omega_r^2 + \frac{\omega_\theta^2}{r^2}\right) + \frac{\omega}{2}\omega_re^{2(\psi-\nu)}(4p_\phi - k_\phi - h_\phi) \\ & + \frac{1}{2}e^{2(\psi-\alpha-\nu)} \left\{ \frac{\omega_r}{2}(2\alpha_\theta + \nu_\theta - 3\psi_\theta)M - \frac{2}{r^2}\omega_\theta\alpha_\theta L + L\omega_r\left(\nu_r - 3\psi_r - \frac{1}{r}\right) \right. \\ & \left. + \frac{1}{r^2}(L_\theta\omega_\theta - M_\theta\omega_r) - L\omega_{rr} - \frac{\omega_{r\theta}}{r^2}M \right\} \quad (\text{A6}) \end{aligned}$$

## B. Angular Derivative Formulae

In this appendix we derive high-order, finite-difference formulae that approximate the angular derivatives of functions that are known at the discrete set of angles  $\mu_i = \cos\theta_i$  (with  $i = 1\dots n$ ), which correspond to the zero's of the Legendre polynomial  $P_{2n-1}(\mu_i) = 0$ . A function  $f(r, \mu)e^{im\phi}$  can be expanded in terms of associated Legendre polynomials as

$$f(r, \mu) = \sum_{k=0}^{\infty} f_k(r) P_{k+|m|}^m(\mu), \quad (\text{B1})$$

Since  $P_{k+|m|}^m$  is a polynomial of order  $k$  multiplied by  $(1 - \mu^2)^{|m|/2}$ , expansion (B1) is equivalent to

$$f(r, \mu) = (1 - \mu^2)^{|m|/2} \sum_{k=0}^{\infty} f_k^\dagger(r) P_k(\mu), \quad (\text{B2})$$

where  $P_k(\mu)$  is the Legendre polynomial of order  $k$ . By orthogonality of the Legendre polynomials, the coefficients  $f_k^\dagger(r)$  in the expansion (B2) are determined as

$$f_k^\dagger(r) = \left(k + \frac{1}{2}\right) \int_{-1}^1 f(r, \mu) (1 - \mu^2)^{-|m|/2} P_k(\mu) d\mu. \quad (\text{B3})$$

The integral in (B3) can be computed with high accuracy using Gaussian quadrature

$$\int_{-1}^1 g^+(r, \mu) d\mu \simeq \sum_{i=1}^n w_i g^+(r, \mu_i), \quad (\text{B4})$$

where  $g^+(r, \mu)$  is a function symmetric in  $\mu$  and  $w_i$  are weights that are tabulated in e.g. Abramowitz & Stegun . For a function  $g^-(r, \mu)$ , antisymmetric in  $\mu$ , the integral in (B4) vanishes.

We are interested in functions  $f(r, \mu)$  that have definite reflection symmetry, i.e. that are of the form  $f^\pm(r, \mu) = \pm f^\pm(r, -\mu)$ . For  $f^+(r, \mu)$ , the nonvanishing coefficients in (B3) become

$$f_{2k}^\dagger = \sum_{i=1}^n \frac{1}{2} (4k + 1) w_i (1 - \mu_i^2)^{-|m|/2} P_{2k}(\mu_i) f^+(r, \mu_i), \quad (\text{B5})$$

while for  $f^-(r, \mu)$ , (B3) yields

$$f_{2k+1}^\dagger = \sum_{i=1}^n \frac{1}{2} (4k + 3) w_i (1 - \mu_i^2)^{-|m|/2} P_{2k+1}(\mu_i) f^-(r, \mu_i). \quad (\text{B6})$$

Differentiating (B2) with respect to  $\mu$  one obtains

$$\begin{aligned} \frac{\partial}{\partial \mu} f^+(r, \mu_i) &= -\frac{|m| \mu_i}{(1 - \mu_i^2)} f^+(r, \mu_i) \\ &+ (1 - \mu_i^2)^{|m|/2} \sum_{k=0}^{\infty} f_{2k}^\dagger(r) \frac{\partial}{\partial \mu} P_{2k}(\mu), \end{aligned} \quad (\text{B7})$$

and substituting (B5) into (B7) yields

$$\frac{\partial}{\partial \mu} f^+(r, \mu_i) = \sum_{j=1}^n D_{ij}^+ f^+(r, \mu_j), \quad (\text{B8})$$

where

$$D_{ij}^+ = -\frac{|m|\mu_i}{(1-\mu_i^2)}\delta_{ij} + (1-\mu_i^2)^{|m|/2} \sum_{k=0}^{n-1} \frac{1}{2}(4k+1)w_j(1-\mu_j^2)^{-|m|/2} P_{2k}(\mu_j) \frac{\partial}{\partial \mu} P_{2k}(\mu_i), \quad (\text{B9})$$

and  $\delta_{ij}$  is the Kronecker delta. Next, we use the recurrence relation

$$\frac{\partial}{\partial \mu} P_{2k}(\mu_i) = \frac{2k}{(1-\mu_i^2)} \left[ -\mu_i P_{2k}(\mu_i) + P_{2k-1}(\mu_i) \right], \quad (\text{B10})$$

in (B9) and define

$$S_{ij}^+ = \sum_{k=1}^{n-1} k(4k+1)P_{2k}(\mu_j) \left[ -\mu_i P_{2k}(\mu_i) + P_{2k-1}(\mu_i) \right]. \quad (\text{B11})$$

In (B9) we truncated the expansion to include Legendre polynomials up to order  $P_{2n-2}(\mu)$ .

If we repeat this for  $f^-(r, \mu)$  and define

$$S_{ij}^- = \sum_{k=0}^{n-2} \frac{(2k+1)}{2}(4k+3)P_{2k+1}(\mu_j) \left[ -\mu_i P_{2k+1}(\mu_i) + P_{2k}(\mu_i) \right], \quad (\text{B12})$$

then  $D_{ij}^\pm$  is given by

$$D_{ij}^\pm = \frac{1}{(1-\mu_i^2)} \left\{ -|m|\mu_i\delta_{ij} + \left[ \frac{1-\mu_i^2}{1-\mu_j^2} \right]^{|m|/2} w_j S_{ij}^\pm \right\}, \quad (\text{B13})$$

and the first-order angular derivative formula becomes

$$\frac{\partial}{\partial \mu} f^\pm(r, \mu_i) = \sum_{j=1}^n D_{ij}^\pm f^\pm(r, \mu_j). \quad (\text{B14})$$

In order to obtain the second-order angular derivatives, we differentiate (B8) with respect to  $\mu$

$$\begin{aligned} \frac{\partial^2}{\partial \mu^2} f^+(r, \mu_i) &= - \left[ \frac{|m|(1 + \mu_i^2) + m^2 \mu_i^2}{(1 - \mu_i^2)^2} \right] f^+(r, \mu_i) - \frac{2|m|\mu_i}{1 - \mu_i^2} \frac{\partial}{\partial \mu} f^+(r, \mu_i) \\ &+ (1 - \mu_i)^{|m|/2} \sum_{k=0}^{\infty} f_{2k}^+(r) \frac{\partial^2}{\partial \mu^2} P_{2k}(\mu_i). \end{aligned} \quad (\text{B15})$$

Differentiating the recurrence relation (B10) with respect to  $\mu$  we obtain

$$\begin{aligned} \frac{\partial^2}{\partial \mu^2} P_{2k}(\mu_i) &= \frac{2k}{(1 - \mu_i^2)^2} \left\{ -[1 + (1 - 2k)\mu_i^2] P_{2k}(\mu_i) \right. \\ &\quad \left. + (3 - 4k)\mu_i P_{2k-1}(\mu_i) + (2k - 1)P_{2k-2}(\mu_i) \right\}. \end{aligned} \quad (\text{B16})$$

Continuing in the same fashion as for the first-order derivatives, we define

$$\begin{aligned} H_{ij}^{\pm} &= \frac{1}{(1 - \mu_i^2)^2} \left\{ -[1 + (1 + |m|)\mu_i^2] |m| \delta_{ij} \right. \\ &\quad \left. - 2|m|\mu_i(1 - \mu_i^2) D_{ij}^{\pm} + \left[ \frac{1 - \mu_i^2}{1 - \mu_j^2} \right]^{|m|/2} w_j G_{ij}^{\pm} \right\}, \end{aligned} \quad (\text{B17})$$

where

$$\begin{aligned} G_{ij}^+ &= \sum_{k=1}^{n-1} k(4k + 1) P_{2k}(\mu_j) \left\{ -[1 + (1 - 2k)\mu_i^2] P_{2k}(\mu_i) \right. \\ &\quad \left. + (3 - 4k)\mu_i P_{2k-1}(\mu_i) + (2k - 1)P_{2k-2}(\mu_i) \right\}, \end{aligned} \quad (\text{B18})$$

and

$$G_{ij}^- = \sum_{k=0}^{n-2} \frac{(2k+1)}{2} (4k+3) P_{2k+1}(\mu_j) \left\{ \begin{aligned} & - (1 - 2k\mu_i^2) P_{2k+1}(\mu_i) \\ & + (1 - 4k)\mu_i P_{2k}(\mu_i) + 2k P_{2k-1} \end{aligned} \right\}. \quad (\text{B19})$$

Then, the second-order angular derivatives for the functions  $f^\pm(r, \mu)$  are

$$\frac{\partial^2}{\partial \mu^2} f^\pm(r, \mu_i) = \sum_{j=1}^n H_{ij}^\pm f^\pm(r, \mu_j). \quad (\text{B20})$$

### C. Perturbed Energy Conservation Equation

In this Appendix, we construct a variational principle for the perturbed energy conservation equation (based on Friedman & Ipser (1992) ) and show its relation to the method presented in section 8. In addition, we derive an explicit expression for the inner product  $\langle \delta U_j | L | \delta U_i \rangle$  defined in section 8.

#### C.1. A Variational Principle

In the Lagrangian formalism, perturbations are described by the Lagrangian displacement vector  $\xi^a$ . The complete description of a perturbation requires the solution of the perturbed field, Euler and energy conservation equations for the metric perturbation  $h_{ab}$  and the displacement vector  $\xi^a$ . If one can solve all but one of the above equations, using for example a trial vector  $\xi^a$ , then the remaining equation will not be satisfied. One then has to construct a criterion, which will be used to identify the equilibrium star for which the remaining equation is satisfied.

For perturbations  $(\xi^a, h_{ab})$  that satisfy the perturbed energy conservation equation

$$\delta(u_b \nabla_a T^{ab}) = 0, \quad (\text{C1})$$

the perturbed field equations form a symmetric system (Friedman & Schutz (1975) ). That is, two pairs  $(\xi^a, h_{ab})$  and  $(\hat{\xi}^a, \hat{h}_{ab})$  satisfying (C1) obey the symmetry relation

$$\hat{\xi}_b \delta(\nabla_c T^{bc}) + \frac{1}{16\pi} \hat{h}_{bc} \delta(G^{bc} - 8\pi T^{bc}) = -\mathcal{L}(\hat{\xi}^a, \hat{h}_{ab}; \xi^a, h_{ab}) + \nabla_b \tilde{R}^b, \quad (\text{C2})$$

where  $G^{ab} = R^{ab} - \frac{1}{2}g^{ab}R_c^c$  and  $\nabla_b \tilde{R}^b$  is a divergence constructed from  $\xi^a$ ,  $\hat{\xi}^a$ ,  $h_{ab}$  and  $\hat{h}_{ab}$ . In (C2),  $\mathcal{L}(\hat{\xi}^a, \hat{h}_{ab}; \xi^a, h_{ab})$  is a function symmetric under the interchange of the trial solutions  $(\xi^a, h_{ab})$  and  $(\hat{\xi}^a, \hat{h}_{ab})$ ; hence the r.h.s. in (C2) is symmetric up to a divergence.

In the Eulerian approach to solving the perturbation equations, the perturbed Euler equation

$$\delta(q^a_b \nabla_a T^{bc}) = 0, \quad (\text{C3})$$

is solved analytically and six components of the perturbed field equation are solved for  $h_{ab}$  given a trial function  $\delta U$ . The symmetry in (C2) can be exploited in order to construct a variational principle for the remaining unsolved equations. The solved perturbed Euler equation can be eliminated from (C2) by decomposing the Lagrangian displacement vector  $\xi^a$  into vectors normal and parallel to the 4-velocity

$$\xi^a = \xi_{\perp}^a - (\xi_c u^c) u^a, \quad (\text{C4})$$

where  $\xi_{\perp}^a = q^a_b \xi^b$ . Equation (C3) then implies

$$\hat{\xi}_b \delta(\nabla_a T^{ab}) = -(\xi_c u^c) \delta(u_b \nabla_a T^{ab}). \quad (\text{C5})$$

For trial solutions the perturbed energy conservation equation is not satisfied

$$\delta(u_b \nabla_a T^{ab}) \equiv L(\delta U) \neq 0, \quad (\text{C6})$$

where  $L$  is a linear operator acting on the function  $\delta U$ .

The Lagrangian displacement  $\xi^a$  has a gauge freedom in its component along  $u^a$ : Adding a vector field  $f u^a$  (where  $f$  is some arbitrary scalar function) to  $\xi^a$  leaves the Eulerian perturbations unchanged. As was shown by Friedman & Ipser (1992), if (C1) is not satisfied, the perturbation equations can still be cast in a symmetric form as in (C2) (but with a redefined divergence term  $\nabla_b \tilde{R}^b$ ) if the component of  $\xi^a$  along  $u^a$  is given the value

$$\begin{aligned} \xi_a u^a &= (u \nabla)^{-1} \delta U \\ &= \frac{1}{i \sigma u^t} \delta U. \end{aligned} \quad (\text{C7})$$

With this definition,

$$\hat{\xi}_b \delta(\nabla_a T^{ab}) = \frac{i \delta \hat{U}}{\sigma u^t} L(\delta U). \quad (\text{C8})$$

Next, we define

$$\begin{aligned} \mathcal{F}(\delta \hat{U}; \delta U) &\equiv \frac{1}{16\pi} \hat{h}_{bc} \delta(G^{bc} - 8\pi T^{bc}) \\ &= \frac{1}{16\pi} (\hat{h}^{bc} - \frac{1}{2} g^{bc} \hat{h}^d{}_d) \delta[R_{bc} - 8\pi(T_{bc} - \frac{1}{2} g_{bc} T^d{}_d)], \end{aligned} \quad (\text{C9})$$

which is implicitly bilinear in  $\delta\hat{U}$  and  $\delta U$ . The gauge freedom in  $h_{ab}$  leaves only six (out of ten) components of the perturbed field equations independent. Thus, if a trial solution satisfies six components of the perturbed field equations in (C9), the other four components of the perturbed field equations will be an implicit functional of the perturbed energy conservation equation, the only remaining equation that needs to be satisfied. Schematically, one can write

$$\mathcal{F}(\delta\hat{U}; \delta U) \equiv \delta\hat{U}\mathbf{F}[L(\delta U)], \quad (\text{C10})$$

where  $\mathbf{F}$  is a functional of  $L(\delta U)$ . We have used the linearity of  $\mathcal{F}(\delta\hat{U}; \delta U)$  to factor out  $\delta\hat{U}$ . The symmetry relation (C2) becomes

$$\begin{aligned} -\mathcal{L}(\hat{\xi}^a, \hat{h}_{ab}; \xi^a, h_{ab}) &= \frac{i\delta\hat{U}}{\sigma u^t} L(\delta U) + \delta\hat{U}\mathbf{F}[L(\delta U)] - \nabla_b \tilde{R}^b \\ &= \delta\hat{U} \left[ \frac{i}{\sigma u^t} + \mathbf{F} \right] L(\delta U) - \nabla_b \tilde{R}^b \\ &\equiv -\mathcal{L}(\delta\hat{U}; \delta U) \end{aligned} \quad (\text{C11})$$

A variational principle for the perturbed energy conservation equation is constructed, by requiring that the following integral (which is implicitly quadratic in  $\delta U$ ) vanishes

$$I = \int -\mathcal{L}(\delta\hat{U}; \delta U) \sqrt{-g} d^3x = 0. \quad (\text{C12})$$

Because the integral of the divergence vanishes, this yields

$$I = \int \delta U \left[ \frac{i}{\sigma u^t} + \mathbf{F} \right] L(\delta U) \sqrt{-g} d^3x = 0. \quad (\text{C13})$$

The integral in (C13) is stationary with respect to first order variations in  $\delta U$

$$\frac{\delta I}{\delta(\delta U)} = 0, \quad (\text{C14})$$

$$\implies \left[ \frac{i}{\sigma u^t} + \mathbf{F} \right] L(\delta U) = 0, \quad (\text{C15})$$

$$\implies L(\delta U) = 0, \quad (\text{C16})$$

provided that  $\frac{i}{\sigma u^t} L(\delta U) \neq -\mathbf{F}[L(\delta U)]$ . Thus,  $I = 0$  is a variational principle for the perturbed energy conservation equation  $L(\delta U) = 0$ .

In practice, one can expand the trial function  $\delta U$  in terms of a set of basis functions  $\delta U_i$

$$\delta U = \sum_i a_i \delta U_i. \quad (\text{C17})$$

Substituting (C17) into (C13) yields

$$\begin{aligned} & \sum_i \sum_j a_i a_j \int \delta U_j \left[ \frac{i}{\sigma u^t} + \mathbf{F} \right] L(\delta U_i) \sqrt{-g} d^3 x = 0 \\ \implies & \sum_i \sum_j a_i a_j A_{(ij)} = 0, \end{aligned} \quad (\text{C18})$$

where we defined the symmetric matrix  $A$  with elements

$$A_{ij} = \int \delta U_j \left[ \frac{i}{\sigma u^t} + \mathbf{F} \right] L(\delta U_i) \sqrt{-g} d^3 x. \quad (\text{C19})$$

Equation (C14) implies that the integral  $I$  will be stationary to the variation of any of the coefficients  $a_i$  in the expansion (C17). Thus,

$$\frac{\delta I}{\delta a_i} = 0 \implies \sum_i a_j A_{(ij)} = 0. \quad (\text{C20})$$

The last equation is a homogeneous linear system for the coefficients  $a_j$  which has a nontrivial solution only when

$$\det A_{(ij)} = 0. \tag{C21}$$

Since we can find an explicit form for  $A_{ij}$  in terms of known quantities, we could have used (C21) as a criterion for locating neutral modes. However, the term  $\mathbf{F}[L(\delta U_i)]$  involves many second order angular and radial derivatives and it is not certain how accurate its evaluation on our finite grid would be. Since the method described in section 8 gives a substantially simpler criterion which does not involve  $\mathbf{F}[L(\delta U_i)]$ , we chose to use that for locating the neutral modes. It is interesting to note that the matrix elements

$$\langle \delta U_j | L | \delta U_i \rangle = \int \frac{i\delta U_j}{\sigma u^t} L(\delta U_i) \sqrt{-g} d^3x \tag{C22}$$

used in section 8 are *nearly* symmetric under the interchange of  $\delta U_i$  and  $\delta U_j$ , for all configurations considered. This indicates that the method described in section 8 nearly coincides with a variational principle.

## C.2. An Expression for the Inner Product

Since for the equilibrium star  $u_b \nabla_a T^{ab} = 0$ ,

$$\begin{aligned} L(\delta U) &= \delta(u_b \nabla_a T^{ab}) \\ &= \Delta(u_b \nabla_a T^{ab}) \\ &= -\Delta[(\epsilon + P)\nabla_b u^b + u^b \nabla_b \epsilon] \\ &= -u^c \nabla_c \left[ \Delta\epsilon + \frac{1}{2}(\epsilon + P)q^{ab} \Delta g_{ab} \right] \end{aligned}$$

$$= -i\sigma u^t \left[ \Delta\epsilon + \frac{1}{2}(\epsilon + P)q^{ab}\Delta g_{ab} \right], \quad (\text{C23})$$

(cf. Friedman & Ipser, 1992). Then,

$$L(\delta U) = -i\sigma u^t \left\{ \delta\epsilon + \xi_{\perp}^a \nabla_a \epsilon + \frac{1}{2}(\epsilon + P) \left[ h_c^c + u^a u^b h_{ab} + 2\nabla_a \xi^a + 2u^a u^b \nabla_a \xi_b \right] \right\}, \quad (\text{C24})$$

where we used  $\Delta g_{ab} = h_{ab} + \nabla_a \xi_b + \nabla_b \xi_a$ . Using the decomposition (C4) of  $\xi^a$ , one obtains

$$\nabla_a \xi^a = \nabla_a \xi_{\perp}^a - \delta U, \quad (\text{C25})$$

and

$$u^a u^b \nabla_a \xi_b = \delta U - \xi_{\perp}^b u^a \nabla_a u_b. \quad (\text{C26})$$

The Euler equations for the equilibrium configuration yield

$$u^b \nabla_b u_c = -\frac{q_c^b \nabla_b P}{\epsilon + P}. \quad (\text{C27})$$

Then (C23) becomes

$$L(\delta U) = -i\sigma u^t \left\{ \delta\epsilon + \xi_{\perp}^a \nabla_a (\epsilon + P) + \frac{1}{2}(\epsilon + P) \left[ h_c^c + u^a u^b h_{ab} + 2\nabla_a \xi_{\perp}^a \right] \right\}. \quad (\text{C28})$$

The perturbed energy density is

$$\delta\epsilon = \frac{(\epsilon + P)^2}{P\Gamma} \left( \delta U + \frac{1}{2} u^a u^b h_{ab} \right), \quad (\text{C29})$$

so that

$$L(\delta U) = -i\sigma u^t \left\{ (\epsilon + P) \left[ \frac{(\epsilon + P)}{P\Gamma} \delta U + \frac{1}{2} \left( 1 + \frac{\epsilon + P}{P\Gamma} \right) u^a u^b h_{ab} + \frac{h_c^c}{2} \right] + \nabla_a [\xi_\perp^a (\epsilon + P)] \right\}. \quad (\text{C30})$$

The matrix elements defined in section 8 now take the form

$$\begin{aligned} \langle \delta U_j | L | \delta U_i \rangle &= \int \frac{i\delta U_j}{\sigma u^t} L(\delta U_i) \sqrt{-g} d^3x \\ &= \int (\epsilon + P) \left\{ \delta U_j \left[ \frac{(\epsilon + P)}{P\Gamma} \delta U_i + \frac{1}{2} \left( 1 + \frac{\epsilon + P}{P\Gamma} \right) u^a u^b h_{ab} + \frac{h_c^c}{2} \right] \right. \\ &\quad \left. - \xi_\perp^a \nabla_a \delta U_j \right\} \sqrt{-g} d^3x, \end{aligned} \quad (\text{C31})$$

where we have used the time-independence of  $\xi^a$  to eliminate the term  $\int \nabla_a [\xi_\perp^a (\epsilon + P) \delta U] \sqrt{-g} d^3x$  as an integral of a spatial divergence.

Finally, the component of  $\xi^a$  normal to the 4-velocity  $u^a$  is related to the component of  $\delta u^a$  normal to  $u^a$  by

$$\xi_\perp^a = \frac{\delta u_\perp^a}{i\sigma u^t} = \frac{\delta u^a - \frac{1}{2} u^b u^c h_{bc} u^a}{i\sigma u^t}, \quad (\text{C32})$$

(cf. Ipser & Lindblom (1992) ) and the expression for  $\langle \delta U_j | L | \delta U_i \rangle$  used in our numerical computations becomes

$$\begin{aligned} \langle \delta U_j | L | \delta U_i \rangle &= \int (\epsilon + P) \left\{ \delta U_j \left[ \frac{(\epsilon + P)}{P\Gamma} \delta U_i + \frac{1}{2} \left( 1 + \frac{\epsilon + P}{P\Gamma} \right) u^a u^b h_{ab} + \frac{h_c^c}{2} \right] \right. \\ &\quad \left. - \frac{(\delta u^a - \frac{1}{2} u^b u^c h_{bc} u^a)}{i\sigma u^t} \nabla_a \delta U_j \right\} \sqrt{-g} d^3x, \end{aligned} \quad (\text{C33})$$

where  $h_{ab}$  and  $\delta u^a$  are computed with  $\delta U_i$ .

Table 1: Comparison of critical configurations in the full and truncated gauges

$N = 1.0$		
$\bar{\epsilon}_c = 0.3$	$T/ W _c$	$\bar{\Omega}_c$
$7 \times 101$		
m=3		
Full gauge	4.63e-2	2.82e-1
Truncated gauge	4.59e-2	2.81e-1
m=4		
Full gauge	3.46e-2	2.48e-1
Truncated gauge	3.47e-2	2.48e-1
m=5		
Full gauge	2.83e-2	2.26e-1
Truncated gauge	2.83e-2	2.26e-1

Table 2: Comparison of critical  $T/|W|$  in Newtonian limit with other authors

	m=3	m=4	m=5
N=1.0			
Present	7.92e-2	5.79e-2	4.62e-2
Managan (1985)	7.94e-2	5.81e-2	—
Imamura <i>et al.</i> (1985)	8.0e-2	5.8e-2	4.4e-2
Ipser & Lindblom (1990)	8.00e-2	5.84e-2	4.53e-2
N=1.5			
Present	5.61e-2	4.33e-2	3.36e-2
Managan (1985)	5.6e-2	4.3e-2	—
Imamura <i>et al.</i> (1985)	5.7e-2	4.3e-2	—
N=2.0			
Present	3.35e-2	2.81e-2	2.28e-2
Managan (1985)	3.3e-2	2.8e-2	—

Table 3: Critical configurations for N=1.0 polytropes

	$\bar{\epsilon}_c$	$T/ W _c$	$(T/ W _c)/$ $(T/ W _K)$	$\bar{\Omega}_c$	$\Omega_c/\Omega_K$
m=2					
Relativistic	3.4e-1	6.49e-2	0.777	3.44e-1	0.911
m=3					
Newtonian	1.0e-8	7.92e-2	0.769	6.69e-5	0.921
Relativistic	3.4e-1	4.55e-2	0.544	2.96e-1	0.783
m=4					
Newtonian	1.0e-8	5.79e-2	0.562	5.94e-5	0.818
Relativistic	3.4e-1	3.53e-2	0.422	2.64e-1	0.699
m=5					
Newtonian	1.0e-8	4.62e-2	0.449	5.41e-5	0.745
Relativistic	3.4e-1	2.87e-2	0.343	2.40e-1	0.635

Table 4: Critical configurations for N=1.5 polytropes

	$\bar{\epsilon}_c$	$T/ W _c$	$(T/ W _c)/$ $(T/ W _K)$	$\bar{\Omega}_c$	$\Omega_c/\Omega_K$
m=3					
Newtonian	1.0e-7	5.61e-2	0.943	1.62e-4	0.980
Relativistic	6.1e-2	3.82e-2	0.804	1.02e-1	0.917
m=4					
Newtonian	1.0e-7	4.33e-2	0.728	1.47e-4	0.886
Relativistic	6.1e-2	2.79e-2	0.587	8.87e-2	0.800
m=5					
Newtonian	1.0e-7	3.36e-2	0.565	1.32e-4	0.796
Relativistic	6.1e-2	2.34e-2	0.492	8.18e-2	0.738

Table 5: Critical configurations for N=2.0 polytropes

	$\bar{\epsilon}_c$	$T/ W _c$	$(T/ W _c)/$ $(T/ W _K)$	$\bar{\Omega}_c$	$\Omega_c/\Omega_K$
m=3					
Newtonian	1.0e-8	3.35e-2	0.991	3.67e-5	0.997
Relativistic	5.1e-3	2.59e-2	0.951	2.22e-2	0.979
m=4					
Newtonian	1.0e-8	2.81e-2	0.832	3.42e-5	0.928
Relativistic	5.1e-3	2.10e-2	0.771	2.02e-2	0.895
m=5					
Newtonian	1.0e-8	2.28e-2	0.676	3.12e-5	0.848
Relativistic	5.1e-3	1.70e-2	0.624	1.84e-2	0.814

## REFERENCES

- Andersson, N. 1997, to appear.
- Abramowitz, M. & Stegun, I. A., *Handbook of Mathematical Functions*, (New York, Dover, 1964)
- Bonazzola, S., Frieben, J. & Gourgoulhon, E. 1996, ApJ, **460**, 379
- Chandrasekhar, S. 1970, Phys. Rev. Lett., **24**, 611
- Cook, G. B., Shapiro, S. L., & Teukolsky, S. A. 1994, ApJ, **424**, 823
- Cutler, C. 1991, ApJ, **374**, 248
- Cutler, C. & Lindblom, L. 1992, ApJ, **385**, 630
- Eriguchi Y., Gourgoulhon E., Nozawa T., Stergioulas N. 1996 (names in temporary order, in preparation).
- Friedman, J. L., & Ipser, J. R. 1992, Phil. Trans. R. Soc. Lond., **A340**, 391
- Friedman, J. L. & Morsink, S. 1997, to appear.
- Friedman, J. L. & Schutz, B. F. 1975, ApJ, **200**, 204
- Friedman, J. L. & Schutz, B. F. 1978a, ApJ, **221**, 937
- Friedman, J. L. & Schutz, B. F. 1978b, ApJ, **222**, 281
- Gropp, W. & Smith, B., in *Proceedings of the Scalable Parallel Libraries Conference* (IEEE,1994) pg. 60
- Imamura, J. N., Friedman, J. L. & Durisen, R. H. 1985, ApJ, **294**, 474
- Ipser, J. R. & Lindblom, L. 1990, ApJ, **355**, 226
- Ipser, J. R. & Lindblom, L. 1991a, ApJ, **373**, 213
- Ipser, J. R. & Lindblom, L. 1991b, ApJ, **379**, 285

- Ipsier, J. R. & Lindblom, L. 1992, ApJ, **389**, 392
- Ipsier, J. R. & Managan, R. A. 1985, ApJ, **292**, 517
- James, R.A. 1964, ApJ, **140**, 552
- Komatsu, H., Eriguchi, Y., & Hachisu, 1989, MNRAS, **239**, 153
- Lindblom, L. 1995, ApJ, **438**, 265
- Lindblom, L. & Mendell, G. 1995, ApJ, **444**, 804.
- Lynden-Bell, D. & Ostriker, J. P. 1967, MNRAS, **136**, 293
- Managan, R. A. 1985, ApJ, **294**, 463
- Priou, D. 1992, MNRAS, **254**, 435
- Regge, T. & Wheeler, J. A. 1957, Phys. Rev. **108**, 1063
- Skinner, D. & Lindblom, L. 1996, preprint, Montana State University
- Stergioulas, N. 1996, “Structure and Stability of Rotating Relativistic Stars,” Ph.D. Thesis,  
University of Wisconsin-Milwaukee.
- Stergioulas, N. & Friedman, J. L. 1995, ApJ **444**, 306
- Weber, F., Glendenning, N. K. & Wiegel, M. K. 1991, ApJ, **373**, 579.
- Yoshida, S. & Eriguchi, Y. 1995, ApJ, **438**, 830
- Yoshida, S. & Eriguchi, Y. 1997, submitted to ApJ Letters.

Fig. 1.— Representative solution for the perturbation functions  $h$  and  $p$  (at  $\phi = 0$ ). Notice that  $p \simeq -h$  even for this very relativistic configuration. The scaling of the vertical axis is determined by the trial function  $\delta U$ . The equator of the star is at  $s = 0.5$ , while  $s = 1.0$  corresponds to infinity. The solution in each figure is shown at  $\mu \equiv \cos \theta = 0, 0.23, 0.45, 0.64, 0.80, 0.92, 0.98$  and  $1.0$ . The maximum is at  $\mu = 0$ .

Fig. 2.— Representative solution for the perturbation functions  $k$  (at  $\phi = 0$ ) and  $\hat{a}$ . Notice that  $k \simeq -h$ . The scaling of the vertical axis is determined by the trial function  $\delta U$ . The equator of the star is at  $s = 0.5$ , while  $s = 1.0$  corresponds to infinity. The solution in each figure is shown at  $\mu \equiv \cos \theta = 0, 0.23, 0.45, 0.64, 0.80, 0.92, 0.98$  and  $1.0$ . The maximum is at  $\mu = 0$ .

Fig. 3.— Representative solution for the perturbation functions  $\hat{L}$  and  $\hat{M}$ . The scaling of the vertical axis is determined by the trial function  $\delta U$ . The equator of the star is at  $s = 0.5$ , while  $s = 1.0$  corresponds to infinity. The solution in each figure is shown at  $\mu \equiv \cos \theta = 0, 0.23, 0.45, 0.64, 0.80, 0.92, 0.98$  and  $1.0$ . For  $\hat{L}$  the maximum is at  $\mu = 0$ . For  $\hat{M}$  the dashed line is at  $\mu = 0.23$  and the maximum is at  $\mu = 0.45$ .

Fig. 4.— Critical angular velocity over Keplerian angular velocity at same central energy density vs. the dimensionless central energy density  $\bar{\epsilon}_c$  for the  $m = 2, 3, 4$  and  $5$  neutral modes of  $N = 1.0$  polytropes. The largest value of  $\bar{\epsilon}_c$  shown corresponds to the most relativistic stable configurations, while the lowest  $\bar{\epsilon}_c$  corresponds to less relativistic configurations. The filled circles on the vertical axis represent the Newtonian limit.

Fig. 5.— Critical ratio of rotational to gravitational binding energy vs. the dimensionless central energy density  $\bar{\epsilon}_c$  for the  $m = 2, 3, 4$  and  $5$  neutral modes of  $N = 1.0$  polytropes. The largest value of  $\bar{\epsilon}_c$  shown corresponds to the most relativistic stable configurations, while the lowest  $\bar{\epsilon}_c$  corresponds to less relativistic configurations. The filled circles on the vertical axis

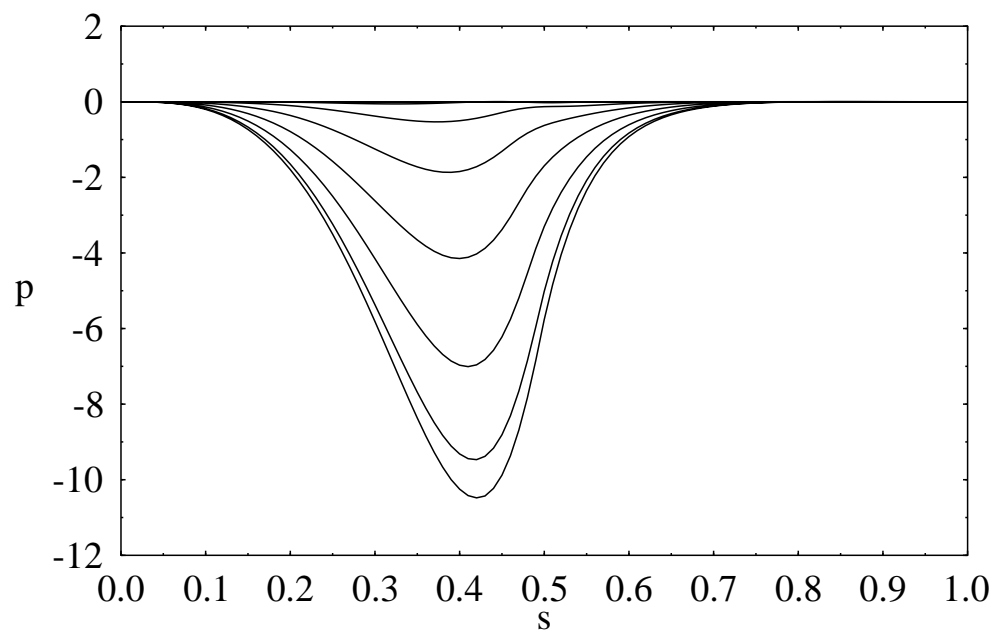
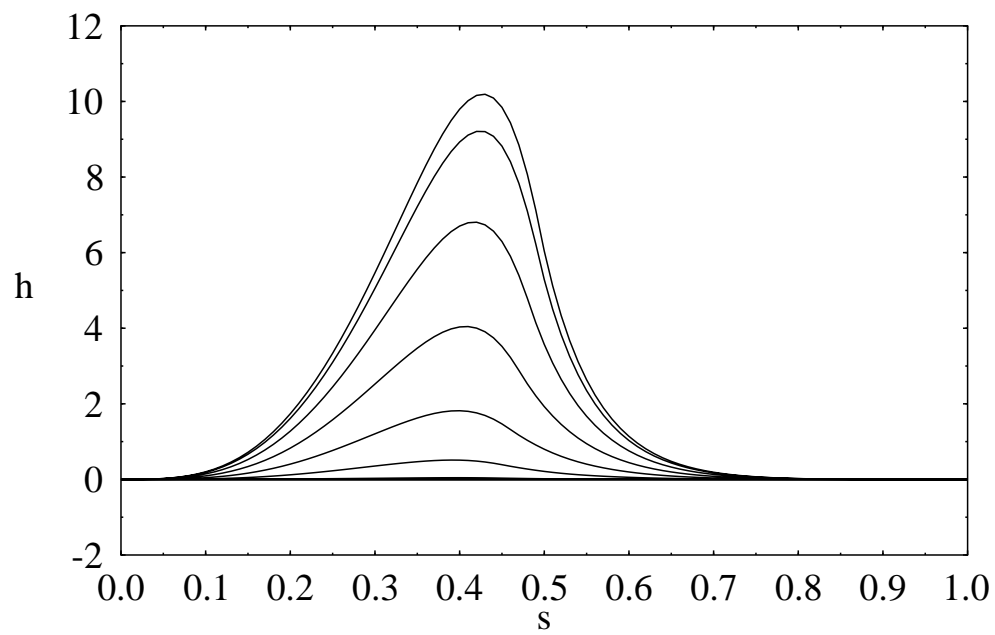
represent the Newtonian limit while the dotted line is the Kepler limit.

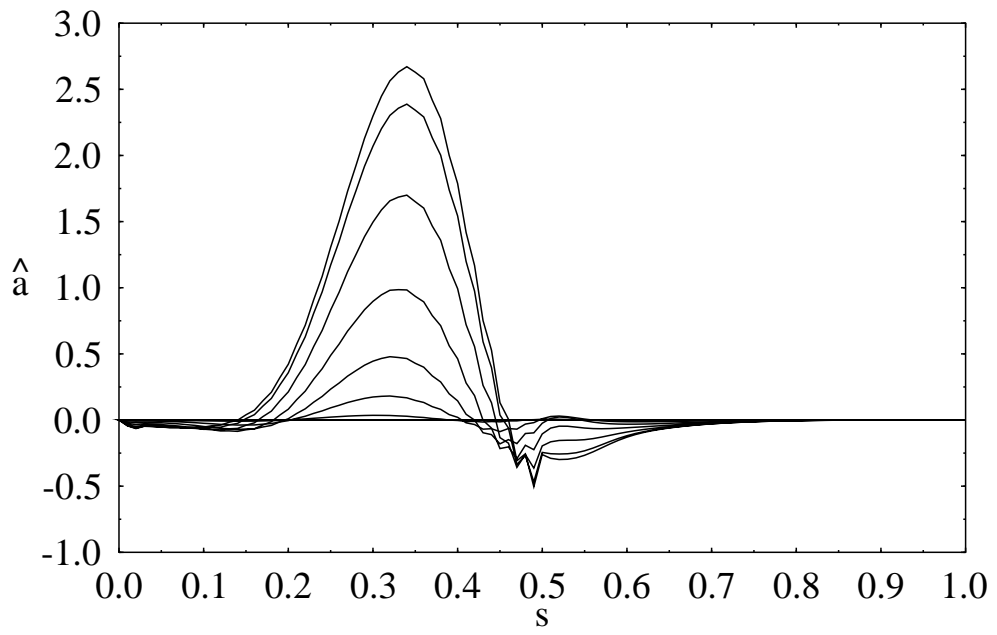
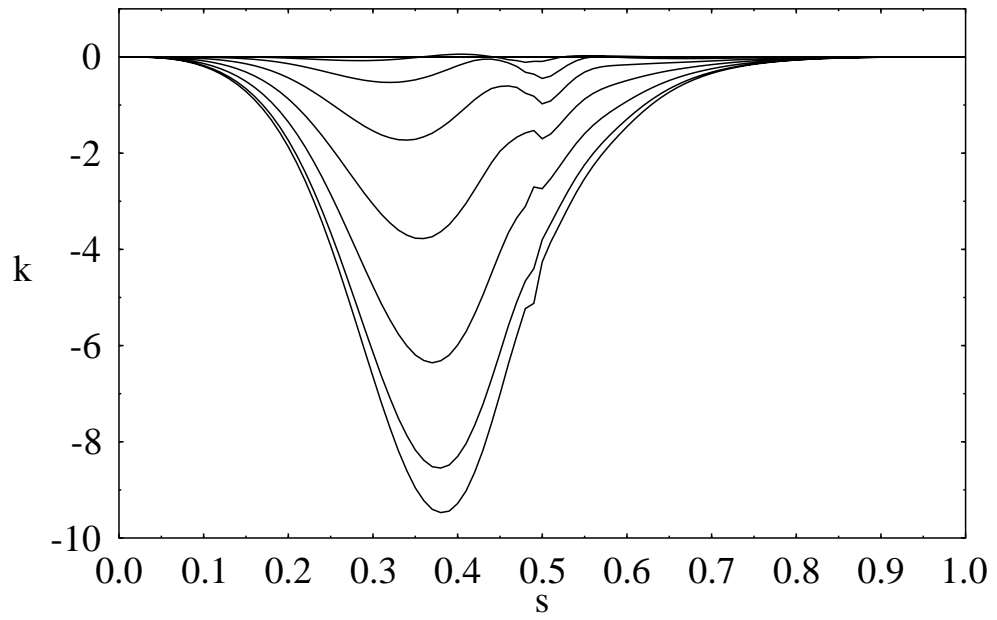
Fig. 6.— Critical angular velocity over Keplerian angular velocity at same central energy density vs. the dimensionless central energy density  $\bar{\epsilon}_c$  for the  $m = 3, 4$  and  $5$  neutral modes of  $N = 1.5$  polytropes. The largest value of  $\bar{\epsilon}_c$  shown corresponds to the most relativistic stable configurations, while the lowest  $\bar{\epsilon}_c$  corresponds to less relativistic configurations. The filled circles on the vertical axis represent the Newtonian limit.

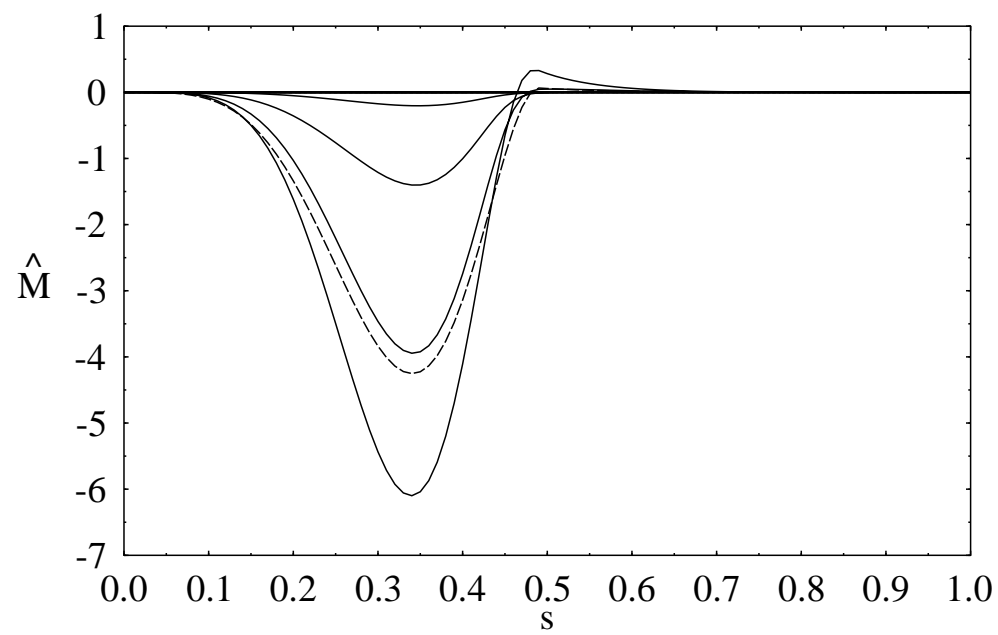
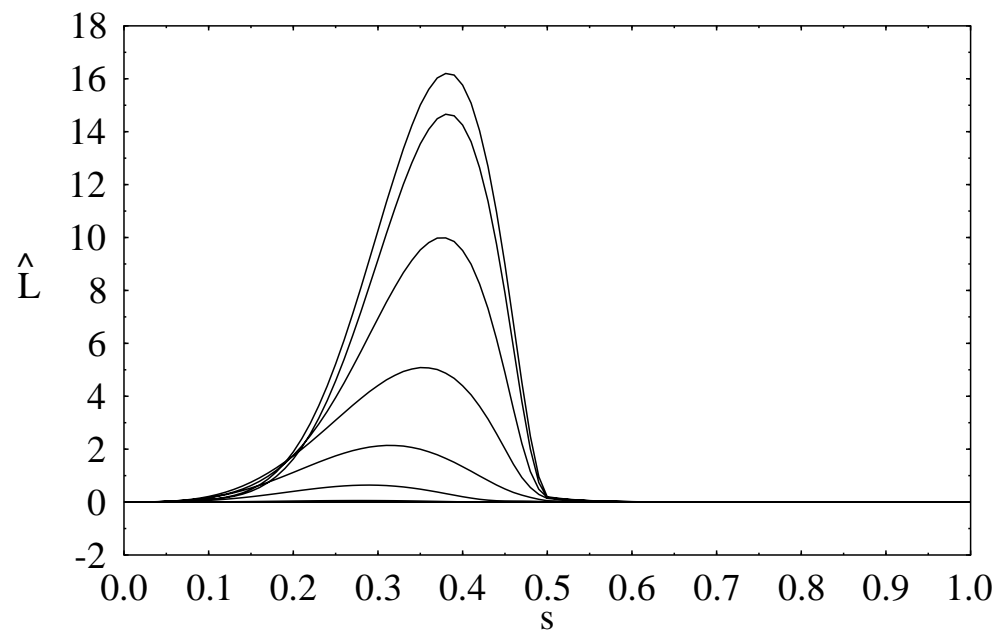
Fig. 7.— Critical ratio of rotational to gravitational binding energy vs. the dimensionless central energy density  $\bar{\epsilon}_c$  for the  $m = 3, 4$  and  $5$  neutral modes of  $N = 1.5$  polytropes. The largest value of  $\bar{\epsilon}_c$  shown corresponds to the most relativistic stable configurations, while the lowest  $\bar{\epsilon}_c$  corresponds to less relativistic configurations. The filled circles on the vertical axis represent the Newtonian limit while the dotted line is the Kepler limit.

Fig. 8.— Critical angular velocity over Keplerian angular velocity at same central energy density vs. the dimensionless central energy density  $\bar{\epsilon}_c$  for the  $m = 3, 4$  and  $5$  neutral modes of  $N = 2.0$  polytropes. The largest value of  $\bar{\epsilon}_c$  shown corresponds to the most relativistic stable configurations, while the lowest  $\bar{\epsilon}_c$  corresponds to less relativistic configurations. The filled circles on the vertical axis represent the Newtonian limit.

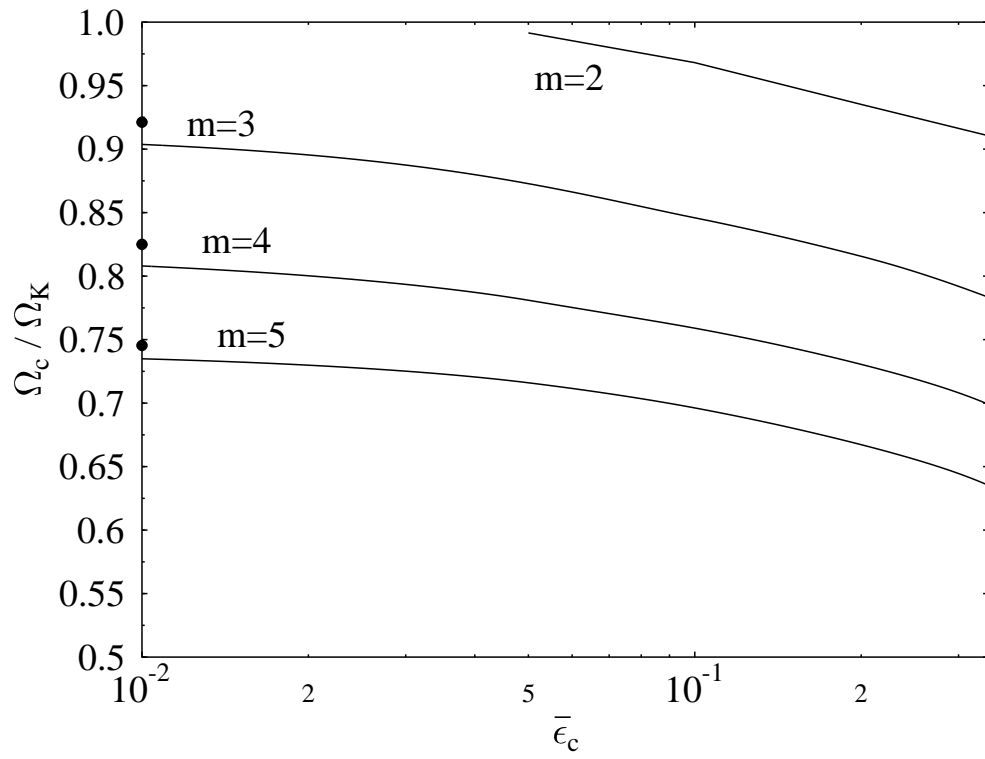
Fig. 9.— Critical ratio of rotational to gravitational binding energy vs. the dimensionless central energy density  $\bar{\epsilon}_c$  for the  $m = 3, 4$  and  $5$  neutral modes of  $N = 2.0$  polytropes. The largest value of  $\bar{\epsilon}_c$  shown corresponds to the most relativistic stable configurations, while the lowest  $\bar{\epsilon}_c$  corresponds to less relativistic configurations. The filled circles on the vertical axis represent the Newtonian limit while the dotted line is the Kepler limit.



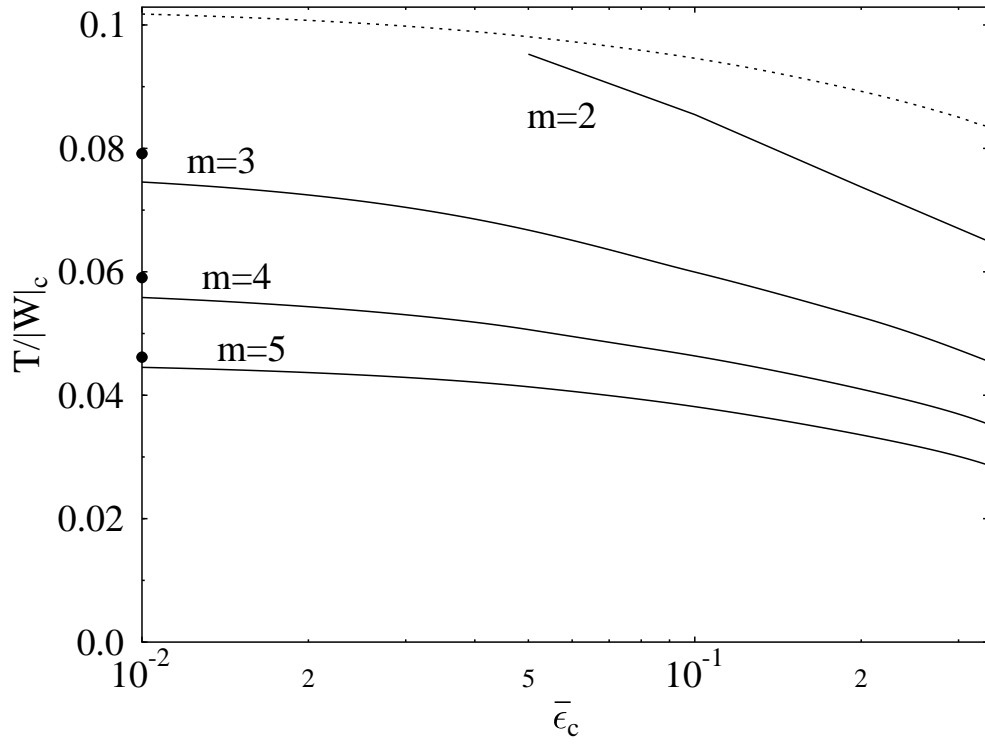




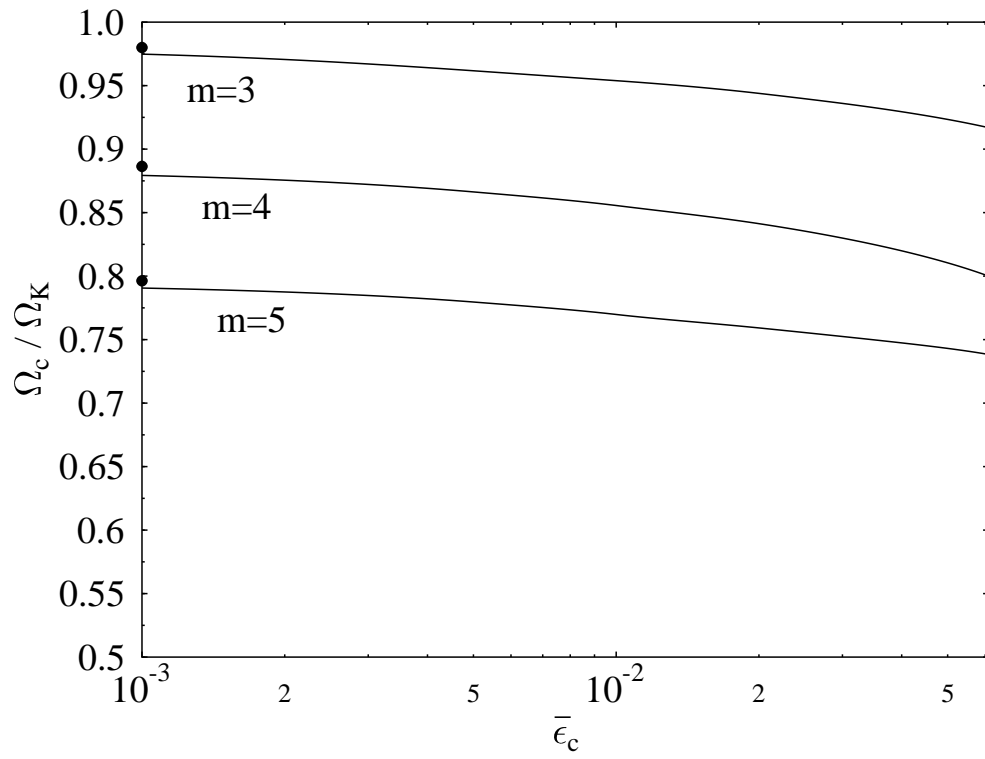
N=1.0



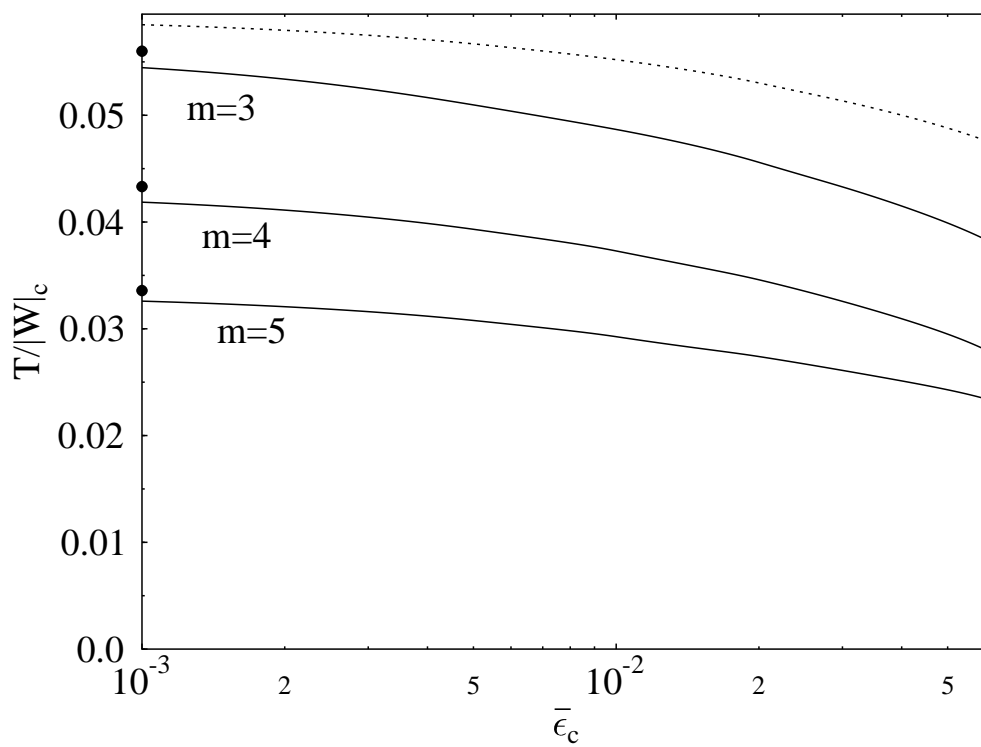
N=1.0



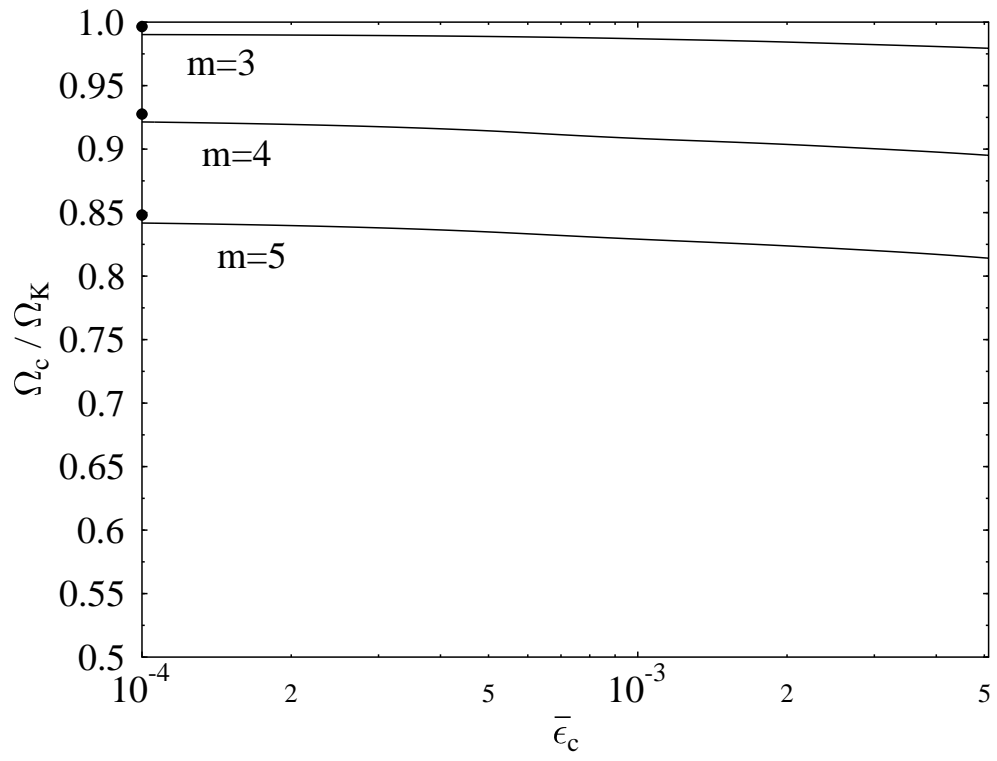
N=1.5



N=1.5



N=2.0



N=2.0

